

Transport across an Anderson quantum dot in the intermediate coupling regime

Johannes Kern* and Milena Grifoni

Institut für Theoretische Physik, Universität Regensburg, 93040 Regensburg, Germany

(Dated: June 17, 2021)

We describe linear and nonlinear transport across a single impurity Anderson model quantum dot with intermediate coupling to the leads, i.e., with tunnel coupling of the order of the thermal energy $k_B T$. The coupling is large enough that sequential tunneling processes alone do not suffice to properly describe the transport characteristics. Upon applying a density matrix approach, the current is expressed in terms of rates obtained by considering a very small class of diagrams which dress the sequential tunneling processes by charge fluctuations. We call this the “dressed second order” (DSO) approximation. One major achievement of the DSO is that, still in the Coulomb blockade regime, it can describe the crossover from thermally broadened to tunneling broadened conductance peaks. When the temperature is decreased even further, the DSO captures “Kondesque” behaviours of the Anderson quantum dot qualitatively: We find a zero bias anomaly of the differential conductance versus applied bias, an enhancement of the conductance with decreasing temperature as well as the onset of universality of the shape of the conductance as function of the temperature. We can address the case of a spin-degenerate level split energetically by a magnetic field and show that, if we assume in addition different capacitive couplings of the two spin-levels to the leads, one of the resonance peaks is vanishing. In case spin-dependent chemical potentials are introduced and only one of the four is varied, the DSO yields *in principle* only one resonance. This seems to be in agreement with experiments with pseudo-spin¹. Furthermore, we get qualitative agreement with experimental data showing a cross-over from the Kondo to the empty orbital regime.

PACS numbers: 73.63.-b, 73.63.Kv

I. INTRODUCTION

The single impurity Anderson model (SIAM)² has become a useful tool to describe phenomena arising in quantum dot devices at low temperatures. It encompasses single-electron tunneling phenomena³, cotunneling and resonant tunneling⁴ as well as Kondo⁵ physics. These phenomena have been verified in many experimental quantum dot set-ups realized at the interface of a two-dimensional electron gas^{6–11}, carbon nanotubes^{12–16} and quantum wires^{17,18} as well as in single-molecule junctions¹⁹. At thermal energies larger than the coupling Γ to the leads transport can be suppressed at low bias due to Coulomb blockade. In this regime sequential tunneling dominates the transport across the SIAM, and tunneling in and out of the dot is well described in terms of rate equations^{20,21}, with rates obtained within a second order perturbation theory in the tunneling Hamiltonian (i.e., first order in Γ). When the temperature is decreased to values of the order of the tunneling coupling Γ or lower, the sequential tunneling approximation breaks down, as processes of higher order in Γ start to become important.

The intermediate coupling regime with tunnel couplings of the order of the thermal energy or higher has not been much investigated so far. This is in part due to the difficulty of developing theories capable to cope with strong Coulomb interactions and intermediate coupling at the same time. However, it is this intermediate regime which might be of interest for transport through some single-molecule junctions^{22,23} and is relevant to interpret experiments on negative tunneling magnetoresistance¹⁴. In the single molecule experiments^{22,23} a conductance gap is observed at low bias which suggests the pres-

ence of charging effects. The gap is followed by conductance peaks whose broadening is larger than the estimated temperature, being a hint that tunneling processes of high order might be responsible for the broadening. In Ref.¹⁴ Coulomb oscillations of the conductance versus the gate voltage are clearly seen in carbon nanotubes contacted to ferromagnetic leads; however, the occurrence of a negative magnetoresistance requires the presence of level shifts due to higher order charge fluctuation processes^{24,25}.

When the temperature is increased even further, one observes the occurrence of a zero bias maximum^{8,26–30} or minimum^{8,31} of the nonlinear conductance for small temperatures in a quantum dot with large Coulomb interaction, depending on whether the single particle resonance lies deep below (Kondo regime) or above (empty-orbital regime) the Fermi level, respectively.

In this paper we describe the transport beyond the sequential tunneling regime by using a diagrammatic approach to the stationary reduced density matrix of the quantum dot and the stationary electron current onto one of the leads. Along the same lines as in Ref.²⁵ we include all possible diagrams which dress the second order tunneling rates by charge fluctuations in and out of the quantum dot. Different from the method in²⁵, we do not only extract tunneling induced level shifts from the analytical expressions. We calculate *transition rates* and express the density matrix and the current in terms of those. Our “dressed second order” (DSO) diagrams are a small subset of the diagrams kept within the so called resonant tunneling approximation (RTA), first proposed by³² to describe the beyond sequential tunneling regime. In particular, for a spinless quantum dot the RTA is exact

and reproduces e.g. the expected Breit-Wigner resonance shape of the linear conductance. The much smaller DSO subset, too, yields the known exact result for the current.

The DSO yields the rates in a straightforward way. We compared the predictions of the RTA and DSO both for the linear and nonlinear conductance in the case of infinitely large Coulomb-repulsion and found only small deviations in the intermediate coupling regime. Larger deviations are seen at lower temperatures where the conductance obtained by the DSO is remaining considerably below the RTA-result.

One major achievement of the DSO is its capability to properly describe a cross-over from thermally broadened conductance peaks at high temperatures to tunneling broadened conductance peaks at low temperatures. This is of relevance e.g. to explain the experiments of Ref.¹⁴. The DSO tunneling rates are given in integral form with the integrand including the product of the density of electron levels and a Lorentzian-like function. Interestingly, a similar form is necessary to ensure convergence of the current in models of quantum dots coupled to superconducting leads³³. Hence, the DSO also provides the minimum diagram selection which yields effective Dynes spectral densities³⁴ in superconducting set-ups.

For small temperatures one expects a zero bias resonance in the transport across a quantum dot with odd occupation and large Coulomb interaction. Both the DSO and the RTA contain this resonance. To test the reliability of the DSO we thus investigated the temperature dependence of the linear conductance obtained by it. We found that there is a temperature T_K such that the conductance is a universal function of the ratio T/T_K . We compared our expression for T_K with results of other theories for the Kondo temperature in the case of infinite Coulomb interaction. Interestingly, as in the RTA³⁵, we find an exponent differing precisely by a factor of two from the result in Ref.³⁶. Moreover, the shape of the conductance curve differs from that expected e.g. from numerical renormalization group predictions.

To show the predictive power of the DSO on a *qualitative* level we address the case that the two spin levels are split energetically by a magnetic field and reproduce the result that the zero bias resonance of the conductance versus the bias splits up into two peaks²⁸. Moreover, we consider the situation that in addition to an energy difference the levels have different capacitive couplings to the contacts (still equal tunneling coupling). In this case we obtain that one part of the double peak vanishes with increasing asymmetry. Measurements which might be explained by this effect were reported in Ref.⁸. Furthermore, we show the behaviour of the DSO-resonance in an unconventional situation: The chemical potentials of the leads depend on the spin. Only one of the four chemical potentials is varied and the others are kept constant and equal. In this situation, the DSO yields only one resonance. Experimental results with a pseudo-spin instead of real spin¹ seem to be in agreement with this

prediction.

Finally, we focus on the case of finite but still large Coulomb interaction and consider the linear conductance as a function of the gate voltage and the temperature. The effect of changing the gate voltage is a shift of the relative position of the level energy with respect to the Fermi level. This offers the possibility to investigate the cross-over from the Kondo regime to the mixed valence and finally the empty orbital regime, corresponding to single particle energies lying deep below, in the vicinity (within an uncertainty of the order of Γ) and above the Fermi level of the leads, respectively. We compare with experimental results in Ref.⁷ and obtain in many respects qualitative agreement.

In summary, despite its simplicity, the DSO provides important insights on the physics of a correlated Anderson quantum dot over a broad regime of parameters. Because the theory is easily scalable to multilevel quantum dots set-ups, it could become an interesting tool to investigate complex quantum dot systems.

The structure of the paper is as follows: Section II introduces the model of the transport current. Section III illustrates the diagrammatic approach and recalls known results for the reduced density matrix and the current in second order in the tunneling Hamiltonian. Analytical expressions for the current and the reduced density matrix are provided in terms of rates.

The DSO approximation is explained in Sec. IV. In Sec. V, VI, and VII the DSO is applied to the spinless case, to the case of infinite interaction and finite interaction, respectively. In particular, in Sec. V and VI the DSO and RTA predictions are compared; the case of energetically split levels is considered. In Sec. VII on the other hand we compare with the experimental results in⁷. Finally, conclusions are drawn in Sec. VIII.

II. BASIC MODEL

A. Hamiltonian

The Hamilton operator of our system is $H = H_R + H_\odot + H_T$. In the reservoirs we assume noninteracting electrons. Correspondingly, we choose

$$H_R = \sum_{l\sigma\mathbf{k}} \varepsilon_{l\sigma\mathbf{k}} c_{l\sigma\mathbf{k}}^\dagger c_{l\sigma\mathbf{k}}.$$

In this formula, the indices l , σ and \mathbf{k} denote the lead, the spin and the wave vector of an electron level in the contacts, respectively; $\varepsilon_{l\sigma\mathbf{k}}$ is the band energy corresponding to this electron level; $c_{l\sigma\mathbf{k}}$ is the annihilation operator of the level $l\sigma\mathbf{k}$ and the dagger denotes the Hermitian conjugate.

The Hamiltonian of the isolated quantum dot is

$$H_\odot = U d_\uparrow^\dagger d_\uparrow d_\downarrow^\dagger d_\downarrow + \sum_\sigma E_\sigma d_\sigma^\dagger d_\sigma,$$

where U is the Coulomb interaction and d_σ and d_σ^\dagger are the annihilation and creation operator of the level $\sigma = \uparrow / \downarrow$ on the dot. Alternatively, the Hamiltonian of the isolated dot can be written as

$$H_\odot = E_0|0\rangle\langle 0| + \sum_\sigma E_\sigma|\sigma\rangle\langle\sigma| + E_2|2\rangle\langle 2|.$$

For any of the four many particle states $a = 0, \uparrow, \downarrow, 2$ we use “ E_a ” to denote the energy of this state. The Hamiltonian of the quantum dot is diagonal in the basis given by these four states. By comparison with the above representation we get: $E_0 = 0, E_2 = U + \sum_\sigma E_\sigma$. Only differences between energies of quantum dot states are relevant. We introduce the terminology

$$E_{ab} := E_a - E_b.$$

Finally, the tunneling Hamiltonian,

$$H_T = \sum_{l\sigma\mathbf{k}} T_{l\mathbf{k}\sigma} d_\sigma^\dagger c_{l\mathbf{k}\sigma} + \text{H. c. (Hermitian conjugate)},$$

connects electron levels on the leads with the level on the quantum dot³⁷. With the term “order” of a tunneling process/ diagram we mean its order in the “tunneling coupling” or “in H_T ”.

B. Initial condition

We assume that there is an initial time at which the systems are still separate and express this by writing the initial density matrix as product of density matrices of the quantum dot and the leads:

$$\rho(t_0) = \rho_\odot(t_0) \otimes \rho_R,$$

where $\rho_\odot(t_0)$ is some arbitrary initial density matrix describing the state of the dot; $\rho_R = \rho_{R,\text{left}} \otimes \rho_{R,\text{right}}$ is the density matrix of the leads in thermal equilibrium. Specifically, we choose

$$\rho_{R,l} = \frac{1}{n_l} \exp\left(\frac{-1}{k_B T} \sum_{\mathbf{k}\sigma} (\varepsilon_{l\mathbf{k}\sigma} - \mu_l) c_{l\mathbf{k}\sigma}^\dagger c_{l\mathbf{k}\sigma}\right),$$

where μ_l is the chemical potential of lead l and where n_l is a normalization factor. After this initial time we assume that the time evolution of the density matrix is ruled by the total Hamiltonian H according to the Liouville-von Neumann equation³⁸ which is the analogon of the Schrödinger equation for density matrices.

C. Thermodynamic limit and the current

For each of the leads we define an electron counting operator as $N_l = \sum_{\mathbf{k}\sigma} c_{l\mathbf{k}\sigma}^\dagger c_{l\mathbf{k}\sigma}$ and the operator of the

particle current onto that lead as $I_l = \frac{i}{\hbar}[H, N_l]$. Then the current onto the chosen lead at time t is

$$\frac{d}{dt} \text{trace}(N_l \rho(t)) = \text{Tr}(I_l \rho(t)) =: \langle I_l \rangle(t).$$

We define the stationary current by letting the time go to infinity and taking the average current:

$$\langle I_l \rangle_\infty = \lim_{\lambda \rightarrow 0} \lambda \int_{t_0}^{\infty} dt \langle I_l \rangle(t) e^{-\lambda(t-t_0)}, \quad (1)$$

where $\lambda > 0$ is the argument of the Laplace transform of the function $\langle I_l \rangle(t)$. The total weight of the multiplicant $\lambda e^{-\lambda(t-t_0)}$ over $[t_0, \infty[$ is always unity, but for smaller and smaller values of λ it will be distributed over a larger and larger time interval. The current in this definition is zero as long as the contacts are finite. Therefore, we first let the size of the contacts go to infinity and re-define

$$\langle I_l \rangle(t) = \lim_{V \rightarrow \infty} \langle I_l \rangle(t, V). \quad (2)$$

Then the current in the definition of Eq. (1) is our model of the dc-current measured in transport experiments with quantum dots.

III. DIAGRAMMATIC APPROACH

A. Basic method

An analysis of the time evolution of the current, Eq. (2), shows that it can be separated into subsequent smallest segments, so-called irreducible tunneling processes^{35,39}. The calculation of the stationary current can be reduced to the calculation of the corresponding transform of these irreducible segments. The theory is exact.

The technical realization of this theory can be described as follows: The irreducible segments of the time evolution of the current are called “kernels”. We distinguish between the “density matrix kernel” K which determines the reduced density matrix of the quantum dot and the “current kernel” K_C which defines the relation between the reduced density matrix and the current. The fact that the time evolution of the current is completely determined by the kernels can be expressed in a compact way by the two equations:

$$\begin{aligned} \langle I_l \rangle(t) &= \text{Tr} \int_{t_0}^t dt' K_C(t-t') \rho_\odot(t'), \\ \dot{\rho}_\odot(t) &= \frac{i}{\hbar} [\rho_\odot(t), H_\odot] + \int_{t_0}^t ds K(t-s) \rho_\odot(s), \end{aligned}$$

where we use the terminology $\rho_\odot(t) := \text{Tr}_R \{\rho(t)\}$ for the reduced density matrix of the quantum dot. The second equation is also called the quantum master equation^{38,40,41}. We take the Laplace transform of both

equations in the limit $\lambda \rightarrow 0$. Then, the second equation allows the calculation of the stationary reduced density matrix as far as $K(\lambda = 0)$ is calculated. Finally, the Laplace transform of the first equation can be used to calculate the stationary current.

The calculation of the current means thus the calculation of the kernels. The contributions to the kernels are visualized by diagrams, whose number and variety is huge. This forces us to take into account only special classes of diagrams about which we have reason to believe that they might be important and which we are able to calculate. Only in the special case of the spinless quantum dot an exact solution was presented³².

B. Second order approximation

Our approximation is an extension of the second order theory, so we recall in the following its meaning and its main predictions.

If we multiply the tunneling Hamiltonian by a dimension-less parameter " w ", then everything becomes a function of w , including the kernels " $K(w)$ ", " $K_C(w)$ " and finally also the current, " $\langle I_l \rangle_\infty(w)$ ". All of the contributions to the kernels have an order in the sense that the coefficients of the tunneling Hamiltonian appear a certain number of times. All odd orders vanish. Thus, they have the structure:

$$\begin{aligned} K(w) &= w^2 K^{(2)} + w^4 K^{(4)} + \dots, \\ K_C(w) &= w^2 K_C^{(2)} + w^4 K_C^{(4)} + \dots \end{aligned}$$

For small values of w , i. e., for weak tunneling coupling, one takes into account only the approximations for the kernels of order $2n$ and calculates the current on this basis. One obtains the current of order $2n$, " $I^{(2n)}(w)$ ", i.e., the Taylor expansion of the current around $w = 0$ of order $2n$. The current, Eq. (1), is analytic in w^2 . In the case $n = 1$ one obtains the second order current, which is just of the form $w^2 \cdot \text{constant}$.

1. Second order density matrix

One of the diagrams visualizing the second order contributions to the density matrix kernel is shown in figure 1. A possible way of describing the process is to say that the quantum dot is at first in the un-occupied state " 0 "; then an electron with spin σ tunnels in two steps onto the dot. Finally, the dot is in the state " σ ". The analytical expressions which correspond to the diagrams are given by diagrammatic rules, e.g.^{31,32,39,42}. The expression for the diagram in Figure 1 reads:

$$\frac{1}{\hbar} \frac{f_l(\varepsilon_{l\mathbf{k}\sigma}) |T_{l\mathbf{k}\sigma}|^2}{\hbar\lambda + i(\varepsilon_{l\mathbf{k}\sigma} - E_{10})},$$

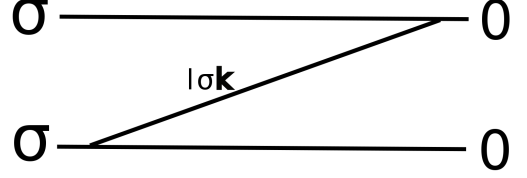


FIG. 1: An example of a second order diagram; by convention we let the time increase from the right to the left. The horizontal lines are called "contours", the third line "tunneling line"; it represents an electron from lead l with spin " σ " and wave vector " \mathbf{k} " which tunnels in two steps onto the dot. The intersection points of the tunneling lines with the contours are called "vertices". The vertices separate the contours into intervals, and to each of these we assign a quantum dot state. The particle number of neighbouring quantum dot states can differ only by ± 1 . The chronological order of the density matrices of the quantum dot in this diagram is found as follows: We imagine a vertical line which cuts each of the contours one time. We consider then especially the intervals between two neighbouring vertices which are cut by the vertical line and take the two quantum dot states assigned to them. If they are " a " and " b " on the lower and on the upper contour, respectively, then the current quantum dot matrix is given by $|a\rangle\langle b|$. The imaginary vertical line we move from the right to the left end of the diagram. The sequence of quantum dot matrices in the above diagram is: $|0\rangle\langle 0|$, $|0\rangle\langle \sigma|$ and finally $|\sigma\rangle\langle \sigma|$.

where we let λ , the argument of the Laplace transform, still be finite. For simplicity we assume degeneracy, $E_\sigma = E_{\bar{\sigma}}$, and write $E_{\sigma 0} =: E_{10}$. Later we will consider also the case of different energies $E_\sigma \neq E_{\bar{\sigma}}$. We let $f_l(\varepsilon)$ be the Fermi function at chemical potential μ_l and temperature T , i.e., $f_l(\varepsilon) = f((\varepsilon - \mu_l)/k_B T)$ with $f(x) = 1/(1 + e^x)$. We perform then the sum with respect to the leads and the wave vector. The thermodynamic limit is taken by replacing the sum with respect to the allowed wave vectors \mathbf{k} by an integral over the first Brillouin zone. The expression turns into:

$$\frac{1}{\hbar} \sum_l \int d\mathbf{k} Z_l \frac{f_l(\varepsilon_{l\mathbf{k}\sigma}) |T_{l\mathbf{k}\sigma}|^2}{\hbar\lambda + i(\varepsilon_{l\mathbf{k}\sigma} - E_{10})},$$

where Z_l is the number of allowed wave vectors in the first Brillouin zone per volume in the wave vector space. We split now the integration into two parts: First, we fix the band energy and integrate over the surface in the first Brillouin zone where $\varepsilon_{l\mathbf{k}\sigma}$ equals this band energy. In a second step, we integrate over the band energies⁴³. The integral turns into:

$$\sum_l \frac{Z_l}{\hbar} \int d\varepsilon \frac{f_l(\varepsilon)}{\hbar\lambda + i(\varepsilon - E_{10})} \int_{\{\varepsilon_{l\mathbf{k}\sigma} = \varepsilon\}} \frac{dS |T_{l\mathbf{k}\sigma}|^2}{|\nabla \varepsilon_{l\sigma}(\mathbf{k})|}.$$

There are two diagrams of second order which are contributions to the "kernel element" $\langle \sigma | \{ K(\lambda) | 0 \rangle \langle 0 | | \sigma \rangle$. They are given by the above diagram and by the one we

get by mirroring this with respect to a horizontal axis. Their contributions are complex conjugate, so we have to take two times the real part of the above expression. In the limit $\lambda \rightarrow 0$ we obtain:

$$\langle \sigma | \{ K(\lambda = 0) | 0 \rangle \langle 0 | \} | \sigma \rangle = \frac{2\pi}{\hbar} \sum_l \alpha_l^+(E_{10}),$$

where we used the notation $\alpha_l^+(\varepsilon) = \alpha_l(\varepsilon) f_l(\varepsilon)$ and

$$\alpha_l(\varepsilon) = \int_{\{\varepsilon_{l\mathbf{k}\sigma} = \varepsilon\}} \frac{dS Z_l |T_{l\mathbf{k}\sigma}|^2}{|\nabla \varepsilon_{l\sigma}(\mathbf{k})|}. \quad (3)$$

In the case that the tunneling coefficients $T_{l\mathbf{k}\sigma}$ were independent of the wave vector the function $\alpha_l(\varepsilon)$ would just be proportional to the density of electron levels in lead l . However, we point out that we do not use such a simplifying assumption about the tunneling coefficients at this stage. The dimension of α_l is “energy”, correspondingly the dimension of the kernel elements is “rate”.

The other second order kernel elements are calculated essentially in the same way. With the further notation $\alpha_l^-(\varepsilon) = \alpha_l(\varepsilon)(1 - f_l(\varepsilon))$ we obtain:

$$\begin{aligned} \langle 0 | \{ K(\lambda = 0) | \sigma \rangle \langle \sigma | \} | 0 \rangle &= \frac{2\pi}{\hbar} \sum_l \alpha_l^-(E_{10}), \\ \langle 2 | \{ K(\lambda = 0) | \sigma \rangle \langle \sigma | \} | 2 \rangle &= \frac{2\pi}{\hbar} \sum_l \alpha_l^+(E_{21}), \\ \langle \sigma | \{ K(\lambda = 0) | 2 \rangle \langle 2 | \} | \sigma \rangle &= \frac{2\pi}{\hbar} \sum_l \alpha_l^-(E_{21}). \end{aligned}$$

For simplicity we assume for this a symmetry in the leads with respect to the spin, i.e., that the definition of α_l , Eq. (3), does not depend on the spin. By considering the contributions of diagrams as in figure 2 one can verify that the general property of the density matrix kernel $Tr \{ K | a \rangle \langle a | \} = 0$ holds true also *within* the second order theory. Therefore, we already calculated implicitly the remaining kernel elements of the form $\langle a | \{ K(\lambda) | a \rangle \langle a | \} | a \rangle$.

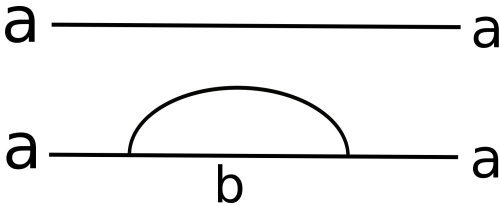


FIG. 2: Second order diagrams of this form ensure that the trace of $K(\lambda) | a \rangle \langle a |$ is always zero. Their contributions to the density matrix kernel amount to $-\sum_{b \neq a} \langle b | \{ K(\lambda) | a \rangle \langle a | \} | b \rangle$.

For the Anderson model quantum dot, the density matrix kernel always transforms a diagonal matrix into a diagonal matrix, i.e., $\langle b | \{ K(\lambda = 0) | a \rangle \langle a | \} | b' \rangle = 0$ if $b \neq b'$.

Thus, we can say that it is a linear operator with rank three or lower acting on the four-dimensional space of the diagonal matrices since one degree of freedom is destroyed by the condition that the trace of the resulting matrix is zero. We can conclude that there is a diagonal solution “ ρ ” of the quantum master equation (QME) in the stationary limit. With the notations

$$\begin{aligned} \rho_{aa} &:= \langle a | \rho | a \rangle, \\ \Gamma_{l,01}^\pm &:= \frac{2\pi}{\hbar} \alpha_l^\pm(E_{10}) \quad \text{and} \\ \Gamma_{l,12}^\pm &:= \frac{2\pi}{\hbar} \alpha_l^\pm(E_{21}) \end{aligned}$$

the QME turns into the following set of two equations (for the three variables ρ_{00}, ρ_{22} and $\rho_{\uparrow\uparrow} = \rho_{\downarrow\downarrow}$):

$$\begin{aligned} 0 &= -\rho_{00} \sum_l \Gamma_{l,01}^+ + \rho_{\sigma\sigma} \sum_l \Gamma_{l,01}^-, \\ 0 &= \rho_{\sigma\sigma} \sum_l \Gamma_{l,12}^+ - \rho_{22} \sum_l \Gamma_{l,12}^-. \end{aligned}$$

This information is sufficient to determine the stationary reduced density matrix since we know that the normalization condition, $\rho_{00} + 2\rho_{\sigma\sigma} + \rho_{22} = 1$, holds. The solution is:

$$\begin{pmatrix} \rho_{00} \\ \rho_{\uparrow\uparrow} \\ \rho_{\downarrow\downarrow} \\ \rho_{22} \end{pmatrix} = \frac{1}{\Gamma_{12}^- \Gamma_{01}^+ + \Gamma_{01}^+ \Gamma_{12}^-} \begin{pmatrix} \Gamma_{01}^- \Gamma_{12}^- \\ \Gamma_{01}^+ \Gamma_{12}^- \\ \Gamma_{01}^+ \Gamma_{12}^+ \\ \Gamma_{12}^+ \Gamma_{01}^+ \end{pmatrix}, \quad (4)$$

where we used the notations

$$\begin{aligned} \Gamma_{ab}^\pm &:= \sum_l \Gamma_{l,ab}^\pm, \\ \Gamma_{ab} &:= \Gamma_{ab}^+ + \Gamma_{ab}^-. \end{aligned}$$

2. Second order current kernel

In order to calculate the current we have to determine the second order current kernel. The structure of the contributions to it is the same as that of the contributions to the density matrix kernel. We take into account only the diagrams with the final vertex on the lower contour. The lead-index attached to the corresponding tunneling line is fixed and given by the lead onto which we are calculating the current. An additional sign, as compared to the density matrix kernel, has then to be taken into account. There are several equivalent possibilities of defining the current kernel³⁵.

For example, the diagram in figure 1 yields the contribution

$$\frac{-1}{\hbar} \int d\varepsilon \frac{\alpha_l^+(\varepsilon)}{\hbar\lambda + i(\varepsilon - E_{10})}$$

to the trace $Tr \{ K_C(\lambda) | 0 \rangle \langle 0 | \}$.

The other contribution to this trace comes from the diagram in figure 2 if we set $a = 0, b = \sigma$. The two contributions are complex conjugate and so we get:

$$\text{Tr} \{K_C(\lambda = 0)|0\rangle\langle 0|\} = -2\Gamma_{l,01}^+.$$

In an analogous way one obtains:

$$\begin{aligned} \text{Tr} \{K_C(\lambda = 0)|2\rangle\langle 2|\} &= 2\Gamma_{l,12}^- \quad \text{and} \\ \text{Tr} \{K_C(\lambda = 0)|\sigma\rangle\langle \sigma|\} &= \Gamma_{l,01}^- - \Gamma_{l,12}^+. \end{aligned}$$

The second order particle current is then found by applying the current kernel to the reduced density matrix and taking the trace³¹:

$$I_l^{(2)}(w = 1) = \frac{2}{N} \begin{pmatrix} \Gamma_{12}^- \\ \Gamma_{01}^+ \end{pmatrix} \begin{pmatrix} \Gamma_{l,01}^+ \Gamma_{l,01} - \Gamma_{l,01}^- \Gamma_{l,01}^+ \\ \Gamma_{l,12}^- \Gamma_{l,12} - \Gamma_{l,12}^+ \Gamma_{l,12}^- \end{pmatrix}, \quad (5)$$

where we used “ \bar{l} ” to denote the opposite lead of lead “ l ” and the abbreviations:

$$\begin{aligned} N &:= \Gamma_{12}^- \Gamma_{01} + \Gamma_{01}^+ \Gamma_{12}, \\ \Gamma_{l,ab} &:= \Gamma_{l,ab}^+ + \Gamma_{l,ab}^-. \end{aligned}$$

The letter w denotes the coupling parameter as introduced above; for simplicity we will leave it away in the following. This is the particle current onto lead l . The net current, i.e., the sum of the two currents onto lead l and \bar{l} , is zero. To determine the electric current one has to multiply by the electron charge.

In the case of proportional tunneling coupling, i.e., $\alpha_l = \kappa_l \alpha$, with κ_l positive scalar factors fulfilling $\sum_l \kappa_l = 1$, the expression for the current can be simplified:

$$\begin{aligned} I_l^{(2)} &= \frac{2}{1 + \frac{\Gamma_{01}^+ \Gamma_{12}}{\Gamma_{01} \Gamma_{12}^-}} \left(\kappa_l \Gamma_{l,01}^+ - \kappa_{\bar{l}} \Gamma_{l,01}^- \right) \\ &+ \frac{2}{1 + \frac{\Gamma_{01} \Gamma_{12}^-}{\Gamma_{01}^+ \Gamma_{12}}} \left(\kappa_{\bar{l}} \Gamma_{l,12}^- - \kappa_l \Gamma_{l,12}^+ \right). \end{aligned} \quad (6)$$

The prefactor of the second line turns out to be the stationary electron number on the quantum dot, i.e., the expectation value $\text{Tr} \{N_{\odot} \rho\}$ with N_{\odot} the particle counting operator on the quantum dot; the prefactor of the first line we might call the “hole number”, i.e., the expectation value of $2 - N_{\odot}$.

The second order approximation can be interpreted in terms of transitions. For every pair of two quantum dot states “ a ” and “ b ” with neighbouring particle numbers and every lead l we determine a rate of transitions “ $a \rightarrow b$ ” caused by the tunneling of an electron from lead l onto the dot or from the dot onto lead l , provided that the dot is in the state $|a\rangle\langle a|$. The stationary density matrix is determined by the demand that all of these transitions compensate each other. Then we calculate the current by balancing the transitions. Our non-perturbative approximation is an extension of the second order theory. The equations for the density matrix and the current in terms of the transition rates $\Gamma_{l,ab}^{\pm}$ still hold true but the expressions for these rates change.

IV. DRESSED SECOND ORDER DIAGRAMS

In this section we account for diagrams similar to the ones of the second order theory but “dress” them by charge fluctuations. Figure 3 shows two possibilities of dressing the second order diagram of figure 1. Apart from the electron that tunnels in two steps onto the dot there is one more electron level of the leads involved. We might say that an electron (lower example diagram) or a hole (upper example diagram) tunnels for some time halfway onto the dot and then leaves it again. For linguistic simplicity we restrict ourselves here to speaking about particles tunneling *onto* the dot, with the consequence that we are using the terms “hole” as well as “electron”. The tunneling of the one electron which finally enters the dot is accompanied by the tunneling of further electrons or holes in these diagrams.

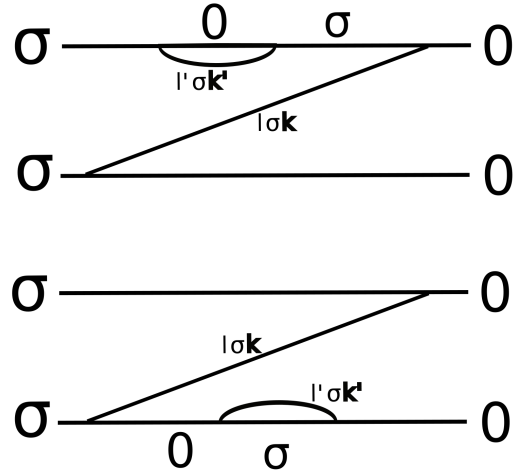


FIG. 3: Two examples of dressing the diagram of figure 1 with further tunneling lines. In the upper diagram the temporal sequence of quantum dot matrices is: $|0\rangle\langle 0|$, $|0\rangle\langle \sigma|$, $|0\rangle\langle 0|$, $|0\rangle\langle \sigma|$ and $|\sigma\rangle\langle \sigma|$. A hole from lead l' with wave vector \mathbf{k}' is participating in the process. In the lower diagram, it is a further *electron* which is accompanying the tunneling of the electron from the level $l\mathbf{k}\sigma$.

According to the diagrammatic rules the sum of the contributions of the diagrams in figure 3 to the density matrix kernel is given by

$$\begin{aligned} &\frac{1}{\hbar} \int d\varepsilon \frac{\alpha^+(\varepsilon)}{\hbar\lambda + i(\varepsilon - E_{10})} \\ &\frac{-1}{\hbar\lambda + i(\varepsilon - E_{10})} \int d\varepsilon' \frac{\alpha(\varepsilon')}{\hbar\lambda + i(\varepsilon - \varepsilon')}, \end{aligned}$$

where we let λ still be finite and used the notations:

$$\begin{aligned} \alpha^{\pm} &:= \sum_l \alpha_l^{\pm}, \\ \alpha &:= \alpha^+ + \alpha^- = \sum_l \alpha_l. \end{aligned}$$

In the first line we recognize the contribution of the second order diagram. However, the integrand is multiplied by a factor, the second line, and this reflects the participation of further particles. From the upper diagram in figure 3 we get " $\alpha^-(\varepsilon')$ ", from the lower one we get " $\alpha^+(\varepsilon')$ ". The sum yields " $\alpha(\varepsilon')$ " which appears in the factor.

Because of the existence of the two spins there is still a third way of dressing our second order diagram with one further tunneling line: The bubble on the lower contour of figure 3 might as well represent an electron with *opposite* spin which accompanies the tunneling. The contribution of this diagram is the same as the contribution of the diagram with only one spin appearing, but it is important because it does not have a counterpart: There is *no way* of dressing the diagram with a bubble on the upper contour which represents a hole of the *opposite* spin. Finally, there is the possibility to dress the diagram by a tunneling line on the upper contour which represents an electron of the opposite spin, as shown in figure 4.

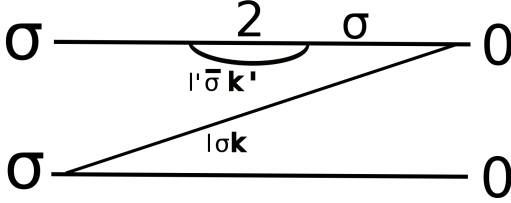


FIG. 4: The existence of the state "2" leads to a fourth possibility of dressing. The tunneling line on the upper contour represents an electron of the opposite spin which tunnels onto the dot and leaves it again.

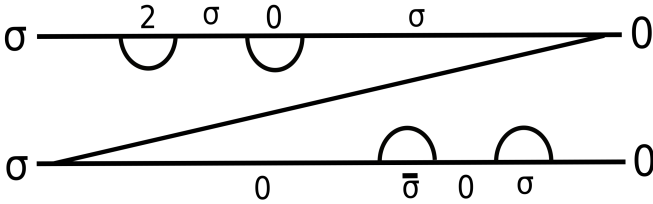


FIG. 5: An example of a diagram with four "bubbles" and one "long" tunneling line. If we count the bubbles from the right to the left, then for the choice of each of them we have essentially four different possibilities. This example-diagram contains all four of these possibilities.

We saw that there are essentially four ways of dressing the second order diagram with one bubble. Moreover, we

can dress the diagrams with two or even more, in general: n , subsequent, non-intersecting, bubbles. An example is sketched in figure 5. For the choice of each of these bubbles we have four possibilities. It might represent an electron of the same or the opposite spin and thus appear on the lower contour or represent a hole of the same spin or an electron of the opposite spin and appear on the upper contour. The sum of the contributions of all of these diagrams to the kernel element $\langle \sigma | \{ K(\lambda) | 0 \rangle \langle 0 | \} | \sigma \rangle$ is

$$\frac{1}{\hbar} \int d\varepsilon \frac{\alpha^+(\varepsilon)}{\eta + i(\varepsilon - E_{10})} \sum_{n=0}^{\infty} \left\{ \frac{-1}{\eta + i(\varepsilon - E_{10})} \right\}^n \\ \left\{ \int d\varepsilon' \frac{(\alpha + \alpha^+)(\varepsilon')}{\eta + i(\varepsilon - \varepsilon')} + \frac{\alpha^+(\varepsilon')}{\eta + i(\varepsilon + \varepsilon' - E_{20})} \right\}^n = \\ \int d\varepsilon \frac{\alpha^+(\varepsilon)/\hbar}{\eta + i(\varepsilon - E_{10}) + \int d\varepsilon' \frac{(\alpha + \alpha^+)(\varepsilon')}{\eta + i(\varepsilon - \varepsilon')} + \frac{\alpha^+(\varepsilon')}{\eta + i(\varepsilon + \varepsilon' - E_{20})}},$$

where we replaced " $\hbar\lambda$ " by " η ". This summation of a geometric series can be justified for "large enough" values of λ . However, we are interested in the limit $\lambda \rightarrow 0$. For this we remember that we want to calculate the Laplace-transform of the sum of the corresponding diagrams in the *time space* and let λ be complex. If the real part of λ is sufficiently large, say, $Re\lambda > c$, then the Laplace transform of the sum of the diagrams in the time space is indeed given by the right hand side of the above equation. One can represent now the sum of the diagrams in the time space as the Laplace back transform of this right hand side⁴⁴ and in this way see that its Laplace transform exists for all values of λ with strictly positive real part. The right hand side of the above equation, *too*, is holomorphic in λ on the whole half plane $\{Re > 0\}$ where the real part is positive. Thus, we have *two* holomorphic functions on $\{Re > 0\}$ which are equal on $\{Re > c\}$. The theory of holomorphic functions says that they must be equal everywhere.

A. DSO tunneling rates

All of the other second order diagrams can be dressed in the same way. For the diagrams connecting the particle numbers one and two we see that a support of the tunneling by holes and electrons of the same spin and by a hole of the opposite spin is possible, but not by an electron of the opposite spin. We obtain the following transition rates within this dressed second order approximation:

$$\Gamma_{l,01}^{\pm} = \frac{2\pi}{\hbar} \int d\varepsilon \frac{\alpha_l^{\pm}(\varepsilon) [(\alpha + \alpha^+)(\varepsilon) + \alpha^+(E_{20} - \varepsilon)]}{\pi^2 [(\alpha + \alpha^+)(\varepsilon) + \alpha^+(E_{20} - \varepsilon)]^2 + [\varepsilon + p_{\alpha+\alpha^+}(\varepsilon) - p_{\alpha^+}(E_{20} - \varepsilon) - E_{10}]^2}, \quad (7)$$

$$\Gamma_{l,12}^{\pm} = \frac{2\pi}{\hbar} \int d\varepsilon \frac{\alpha_l^{\pm}(\varepsilon) [(\alpha + \alpha^-)(\varepsilon) + \alpha^-(E_{20} - \varepsilon)]}{\pi^2 [(\alpha + \alpha^-)(\varepsilon) + \alpha^-(E_{20} - \varepsilon)]^2 + [\varepsilon + p_{\alpha+\alpha^-}(\varepsilon) - p_{\alpha^-}(E_{20} - \varepsilon) - E_{21}]^2}, \quad (8)$$

where we define for any function h the function p_h by

$$p_h(\varepsilon) := \int d\omega \frac{h(\varepsilon + \omega) - h(\varepsilon - \omega)}{\omega}. \quad (9)$$

Hence, the DSO rates are given in the form of an integral where the integrand is the product of the second order functions $\alpha_l^{\pm}(\varepsilon)$ and of a Lorentzian-like resonance function. We thus expect that the second order rates are recovered when the temperature broadening of the functions α_l^{\pm} largely exceeds the width of the Lorentzian broadening. In the limit of weak coupling these transition rates indeed turn into the transition rates of the second order theory. More precisely, we get if we multiply the tunneling Hamiltonian with a parameter w as done in III B:

$$\frac{\Gamma_{l,ab}^{\pm}(\text{dressed second order})(w)}{\Gamma_{l,ab}^{\pm}(\text{second order})(w)} \rightarrow 1(w \rightarrow 0).$$

The stationary reduced density matrix within the DSO is given by Eq. (4) and the current is given by Eq. (5) and in the case of proportional coupling by Eq. (6).

In Ref.³¹ a diagram selection called the "resonant tunneling approximation" (RTA) was applied: The case of infinite interaction was considered and therefore the diagrams containing the state "two" do not contribute; transition rates were derived, the stationary density matrix was determined and finally the current was obtained.

The RTA takes into account all of the diagrams within the DSO which do not contain the state "2". However, there are many diagrams outside the DSO which are contained in the RTA as we will discuss in Sec. V. Comparisons between the predictions of the DSO and RTA will be performed in the cases of the spinless quantum dot and of the SIAM with infinite interaction.

B. Linear conductance within the DSO

We assume that we can obtain the second order functions α_l by multiplication of the density of electron levels in the leads by a coupling constant while in general their definition is more complicated (Eq. (3)). About the density of electron levels we make simplifying assumptions such that we can concentrate on effects which are not due to special behaviour of the density of electron levels. In particular, we place the Fermi level in a point with respect to which the density of electron levels is symmetric. Then the chemical potential at equilibrium coincides with the Fermi level for all temperatures, see figure 7. By deriving the formula for the current, Eq. (6), with respect to the bias, $eV_{bias} = \mu_l - \mu_{\bar{l}}$, one obtains at zero bias the following expression for the linear conductance:

$$G^{(DSO)} = 4\kappa_l \kappa_{\bar{l}} \frac{e^2}{h} \left(\frac{(2 - n_{\odot})|^{V_{bias}=0}}{n_{\odot}|^{V_{bias}=0}} \right) \left(\frac{\int d\varepsilon \frac{\pi^2 \alpha(\varepsilon) [(\alpha + \alpha^+)(\varepsilon) + \alpha^+(E_{20} - \varepsilon)]}{d_{01}(\varepsilon)}}{\int d\varepsilon \frac{\pi^2 \alpha(\varepsilon) [(\alpha + \alpha^-)(\varepsilon) + \alpha^-(E_{20} - \varepsilon)]}{d_{12}(\varepsilon)}} \right) \bigg|_{V_{bias}=0}^{\frac{-1}{k_B T} f' \left(\frac{\varepsilon - E_F}{k_B T} \right)}, \quad (10)$$

where E_F is the Fermi level, $f(x) = 1/(1 + e^x)$ the normalized Fermi function,

$$n_{\odot} = \frac{2}{1 + \frac{\Gamma_{01}\Gamma_{12}^-}{\Gamma_{01}^+\Gamma_{12}^+}}$$

is the particle number on the dot as noted above, and where we use the abbreviations " $d_{01}(\varepsilon)$ " and " $d_{12}(\varepsilon)$ " for the denominators in the expressions for the transition

rates, Eqs. (7) and (8), respectively. The prefactor $4\kappa_l \kappa_{\bar{l}}$ is one in the case of symmetric coupling and less than one otherwise. We finally included the electron charge into the formula.

V. RESULT OF THE DSO FOR A SPINLESS QUANTUM DOT

We consider here the case of a spinless quantum dot with only two possible states "0" and "σ", so with only one spin. One obtains it by not performing the sum with respect to the spin in the Hamiltonian. This problem is equivalent to the SIAM with $E_{\uparrow} = E_{\downarrow}$ and $U = 0$ in the sense that current across the SIAM quantum dot is then just two times the current across a spinless quantum dot.

The contribution of all diagrams outside the RTA to the kernels is zero⁴⁵ for the spinless quantum dot and thus, the RTA is exact in this case. The relation between our approximation and the diagrams of the RTA is described by figure 6. In the case of the spinless quantum dot treated here as well as in the case of infinite interaction the figure characterizes the relation between the diagram selections completely.

The DSO approximation concentrates on the second order diagrams dressed by further tunneling lines, the RTA takes these ones in order to construct even more diagrams. The resulting diagrams are a combination of an integer number of DSO-diagrams. The transition rates of the DSO in the case of the spinless quantum dot we get by taking into account only those diagrams within the DSO which contain only the quantum dot states "0" and "σ":

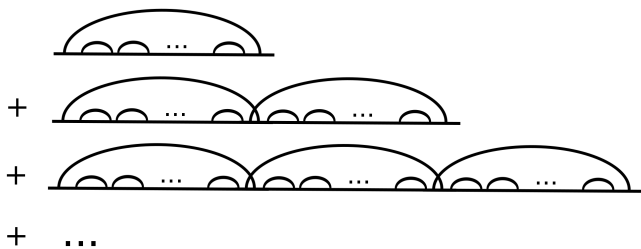


FIG. 6: The structure of the diagrams within the RTA. When projecting all of the tunneling lines onto one contour only, the first line shows the diagrams within the DSO; in the following lines, two, three, in general: n diagrams of this kind are combined to create new ones out of them. For the sum of all of these diagrams, an integral equation was derived³². Its origin is the relation between the contributions of all combinations of n or less diagrams of the DSO on the one hand and of all combinations of $n + 1$ or less DSO-diagrams on the other hand. In the limit $n \rightarrow \infty$ the two are equal.

$$\Gamma_{l,01}^{\pm} = \frac{2\pi}{\hbar} \int d\varepsilon \frac{(\alpha_l^{\pm} \alpha)(\varepsilon)}{\pi^2 \alpha^2(\varepsilon) + (p_{\alpha}(\varepsilon) + \varepsilon - E_{10})^2}.$$

We get the density matrix

$$\begin{pmatrix} \rho_{00} \\ \rho_{11} \end{pmatrix} = \frac{1}{\Gamma_{01}^{+} + \Gamma_{01}^{-}} \begin{pmatrix} \Gamma_{01}^{-} \\ \Gamma_{01}^{+} \end{pmatrix}$$

and the particle current in the case of proportional cou-

pling:

$$I_l^{DSO} = 4\kappa_l \kappa_{\bar{l}} \frac{\pi^2}{\hbar} \int d\varepsilon \frac{\alpha^2(\varepsilon) (f_{\bar{l}} - f_l)(\varepsilon)}{\pi^2 \alpha^2(\varepsilon) + (\varepsilon + p_{\alpha}(\varepsilon) - E_{10})^2}.$$

In the limit of small temperatures and in case the second order functions $\alpha_l(\varepsilon)$ are rather constant the current is obtained by integrating a Lorentzian-like function with width (full width at half maximum) $\Gamma := 2\pi\alpha$ between the two chemical potentials. The differential conductance as function of the bias thus reproduces the shape of this Lorentzian. Frequently, the quantity Γ rather than α is used to define the coupling.

In the case of proportional tunneling coupling the result of the DSO for the spinless quantum dot is actually the *same* which was presented within the RTA³² and thus exact. In the case of non-proportional tunneling coupling the results become different.

The diagram selection defined by the first line in figure 6 we might call the "simple" selection since the pair formation of $2n$ subsequent times is one of the simplest possible irreducible pair formations. In the case of finite interaction the DSO diagram selection contains *less* diagrams than the simple selection. The DSO for finite U does not describe the noninteracting limit, where $U = 0$, correctly. This can be seen by comparing the formulas for the linear conductances of the DSO in case $U = 0$ on the one hand and of the DSO in the spinless case on the other hand. However, we know by now that the *simple* diagram selection *does* describe the noninteracting limit correctly. Moreover, the simple selection seems to suggest the natural way to extend the RTA to the case of finite U , even though the diagram summation might be technically difficult. The simple selection we want to discuss elsewhere. We will now concentrate on applying the DSO approximation to cases with nonzero interaction. We will consider the regimes $\Gamma \sim k_B T$ and $\Gamma \gg k_B T$ and ask with respect to which aspects the DSO is successful in explaining experimental results and how it compares with existing theories.

VI. THE CASE OF INFINITE INTERACTION

In the case of infinite interaction, $U = \infty$, it makes sense to neglect all of the diagrams which contain the state "2", assuming $\rho_{00} + \sum_{\sigma} \rho_{\sigma\sigma} = 1$. This was done within the RTA and a result for the current was derived³¹. One can do the same with the DSO. The formulas for the linear conductance of the RTA and DSO in

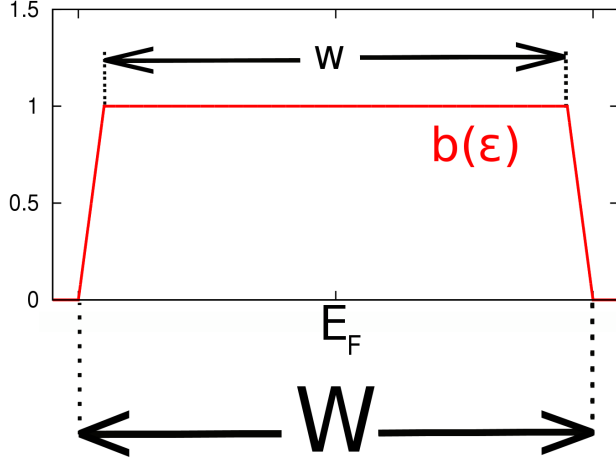


FIG. 7: Energy dependence of the dimensionless function $b(\varepsilon) = \alpha(\varepsilon)/\alpha(E_F)$. We placed the Fermi level E_F in the middle in order to ensure that the chemical potential at equilibrium always equals the Fermi level. Moreover, we chose $W = 1\text{eV}$, $w = 0.9W$. A cut-off is needed in order to ensure the existence of the principal parts p_α, p_{α^+} etc. of Eq. (9).

the “ $U = \infty$ case” read:

$$G^{RTA} = 4\kappa_l\kappa_{\bar{l}}\frac{e^2}{h}2 \int d\varepsilon \frac{\pi^2\alpha^2(\varepsilon)}{d(\varepsilon)} \frac{-1}{k_BT} f' \left(\frac{\varepsilon - E_F}{k_BT} \right),$$

$$G^{DSO} = 4\kappa_l\kappa_{\bar{l}}\frac{e^2}{h} (2 - n_\odot) \int d\varepsilon \frac{\pi^2 [\alpha(\alpha + \alpha^+)](\varepsilon)}{d(\varepsilon)} \frac{-1}{k_BT} f' \left(\frac{\varepsilon - E_F}{k_BT} \right),$$

where we used the abbreviation $d(\varepsilon) := \pi^2(\alpha + \alpha^+)^2(\varepsilon) + (\varepsilon + p_{\alpha+\alpha^+}(\varepsilon) - E_{10})^2$ for the common denominator. Differences are only found in the prefactor and in the numerator. To compute the conductances we have to make a choice about the second order function $\alpha(\varepsilon)$. We wrote $\alpha(\varepsilon) = \alpha(E_F) \cdot b(\varepsilon)$ with a dimensionless function $b(\varepsilon)$ fulfilling $b(E_F) = 1$. The variable $\alpha(E_F)$ is then our coupling parameter. Figure 7 shows how we chose the function $b(\varepsilon)$.

A. Coulomb peaks from high to low temperatures

In figure 8 we compare the linear conductances as a function of the gate voltage obtained within the RTA and the DSO for various temperatures. We observe a transition from a temperature dominated to a tunneling dominated width of the Coulomb peak. The transition occurs at temperatures around 1K which corresponds to a thermal energy which is of the order of the chosen coupling $\alpha(E_F) = 0.042\text{meV}$. The peak height of the DSO still increases up to temperatures of about 100mK

and decreases then. In this respect, the DSO fails to describe experimental reality below 100mK . Notice that the shape of the curve saturates at low temperatures both within the RTA and the DSO: the effect of decreasing the temperature further and further is only a shift of the graph. As we will show in the next subsection, these features do not depend on the choice of $b(\varepsilon)$.

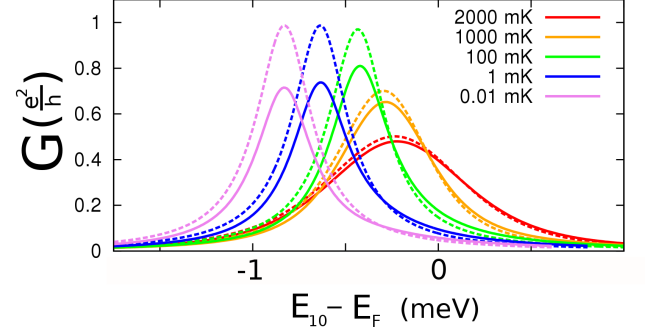


FIG. 8: (Colour online.) Linear conductance of the DSO as a function of the energy difference E_{10} for different temperatures. The dashed lines show the result of the RTA; the coupling we chose to be $\alpha(E_F) = 0.042\text{meV}$ and $W = 1\text{eV}$. (The same choices we made for a later comparison with an experiment, discussed in Sec. VII B.) A temperature of 1K corresponds to a thermal energy of about $k_BT \approx 0.1\text{meV}$. For large temperatures the resonance is smeared out, its centre is found roughly around the Fermi level. For decreased temperatures the position of the maximum is shifted and the width of the peak is proportional to $\alpha(E_F)$. While the logarithmic shift of the peak with the temperature does not stop, the shape of the curve and its maximum value saturate. We find numerically within the RTA the maximum $\approx 0.99e^2/h$, within the DSO $\approx 0.69e^2/h$. We emphasize that neither these maximum values nor the shapes of the curves in the limit of small temperatures depend on the way in which the function $b(\varepsilon)$ is chosen.

B. Universality and Kondo temperature in the infinite U -case

We show now that the DSO conductance displays universality as function of the temperature in the regime of strong coupling. For a fixed value of the gate voltage, i.e., for fixed E_{10} , the linear conductance becomes a function “ $G(T)$ ” of the temperature. This is expected to display universality⁴⁶ in the following sense: There is a temperature T_K such that $G(T)/G_{max}$ is a universal function of the ratio T/T_K , where G_{max} is the maximum value of the conductance. This statement we can show about G^{DSO} as well as about G^{RTA} . Both the RTA and the DSO, however, do not yield the expected convergence of $G(T) \rightarrow G_{max} = 4\kappa_l\kappa_{\bar{l}} \cdot 2e^2/h$ ($T \rightarrow 0$).

As we will show in the appendix one can represent

G^{DSO} in the form

$$G^{DSO} \approx 4\kappa_l \kappa_{\bar{l}} \frac{e^2}{h} (2 - n_{\odot}) F^{DSO} \left(\frac{E_{10} - \bar{E}_{10}}{\alpha(E_F)}, \frac{k_B T}{\alpha(E_F)} \right),$$

where the definition of F^{DSO} is

$$F^{DSO}(a, b) = \int dx \frac{-\pi^2 f'(x)(1 + f(x))}{\pi^2 (1 + f(x))^2 + \phi_{a,b}^2(x)}$$

and where

$$\bar{E}_{10} = E_F + \alpha(E_F) p_{b_T^+} (E_F).$$

Finally, the function $\phi_{a,b}(x) = g(x) - a + xb + \log(b)$ is defined by the use of Eq. (17). The temperature $T_{\alpha(E_F)}$ we define by the demand $k_B T_{\alpha(E_F)} = \alpha(E_F)$. The function $b_T^+(\varepsilon)$ is given by $b_T^+(\varepsilon) = b(\varepsilon) f((\varepsilon - E_F) k_B T)$.

The particle number n_{\odot} is a function of the tunneling rates and still contains the temperature. However, for temperatures $k_B T \ll \alpha(E_F)$ these become essentially independent of the temperature such that we can concentrate on the temperature dependence of the rest. The integral with respect to x contains the derivative of the Fermi function and is thus concentrated in a region of the order of one around zero. Therefore, we can in the case of small temperatures compared to $\alpha(E_F)$, $k_B T \ll \alpha(E_F)$, neglect the linear term in $\phi_{a,b}(x)$ and estimate

$$\phi_{a,b}(x) \approx g(x) - a + \log(b).$$

The simplification enables us to write

$$G^{DSO} \approx 4\kappa_l \kappa_{\bar{l}} \frac{e^2}{h} (2 - n_{\odot}) F^{DSO} \left(-\frac{E_{10} - \bar{E}_{10}}{\alpha(E_F)} + \log \frac{T}{T_{\alpha(E_F)}} \right),$$

with

$$F^{DSO}(c) = \int dx \frac{-\pi^2 f'(x)(1 + f(x))}{\pi^2 (1 + f(x))^2 + (g(x) + c)^2}.$$

For large positive values of c , $F^{DSO}(c)$ takes small positive values. At some value " c_{max} " a maximum is reached. In between there is a value of c , " $c_{1/2}$ ", where we have $F^{DSO}(c_{1/2}) = 0.5 F^{DSO}(c_{max})$.

We define the Kondo temperature by the demand $c = c_{1/2}$, i.e.,

$$T_K := e^{c_{1/2}} \exp \left(\frac{E_{10} - E_F}{\alpha(E_F)} \right) T_{\alpha(E_F)} \exp \left(-p_{b_T^+} (E_F) \right).$$

The second line seems to depend on the coupling $\alpha(E_F)$, but this dependence is weak because of the logarithmic dependence of $p_{b_T^+}(E_F)$ on the temperature which we

show in the appendix. The dependence on the bandwidth W as introduced in figure 7 is proportionality as long as $\alpha(E_F) \ll W$ such that we arrive at

$$k_B T_K = 7W \exp \left(\frac{E_{10} - E_F}{\alpha(E_F)} \right) \quad (11)$$

after numerical evaluation of the constants. The prefactor, in our case "7", changes if shape of the band (figure 7) is chosen in a different way, for example, to be Lorentzian. The rest of the derivation is independent of the choice of the coupling function.

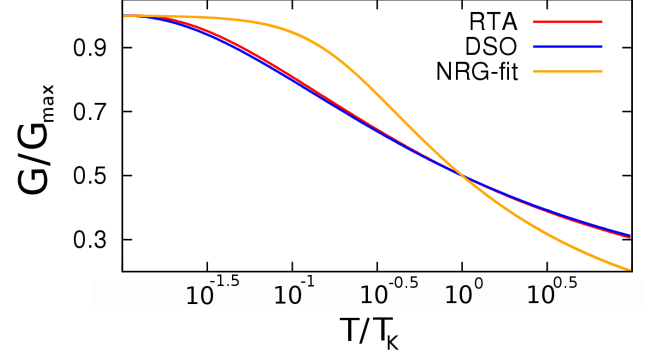


FIG. 9: A comparison of the universal function of the DSO with an NRG-fit⁷. Both functions take the value 0.5 at $T = T_K$ and are normalized in such a way that the maximum is one. A striking feature of the fit is that within one power of ten the linear conductance goes up from 50 % to about 95 % of its maximum while our function is growing much less in this interval. We included also the universal curve which one gets for the RTA. In agreement with figure 8 and unlike the NRG-fit, the universal functions of RTA and DSO are going down again for even smaller exponents than shown here. The equation for the NRG-fit is $G(T) = G_{max} (1 / [(T/T_K')^2 + 1])^s$ with $T_K' = T_K / (2^{1/s} - 1)^{1/2}$ so that $G(T_K) = G_{max}/2$; we chose $s = 0.2$.

We summarize the conditions for which the done simplifications are valid:

$$k_B T \ll \alpha(E_F) \ll W.$$

Then we can represent

$$G^{DSO} = 4\kappa_l \kappa_{\bar{l}} \frac{e^2}{h} (2 - n_{\odot}) F^{DSO} \left(c_{1/2} + \log \frac{T}{T_K} \right),$$

where T_K is given by Eq. (11). The linear conductance becomes a universal function of T/T_K ; at $T = T_K$, $G(T)$ reaches one half of its maximum. In figure 9 we compare our result for the universal function with a fit to the one obtained by NRG-calculations⁴⁶. Essentially the same arguments one can apply to the RTA in order to obtain an analogous universality; the formula for T_K deviates only in the prefactor. The relation between $\alpha(E_F)$ and the coupling parameter " Γ " by the use of which T_K is most frequently expressed, e.g.^{7,29,35}, is $\Gamma = 2\pi\alpha(E_F)$.

We acknowledge very clearly that the DSO fails to describe the regime of strong coupling quantitatively correctly. However, we think it is very remarkable that the linear conductance obtained by it displays a universality *in the same sense* as it is predicted by perfectly different theories.

C. Zero bias anomaly of the differential conductance

In addition to the linear conductance we considered the differential conductance obtained within the infinite-

U DSO. We notice that in qualitatively the same way as the RTA³¹ the approximation produces a zero bias maximum of the differential conductance in case E_{10} lies below the Fermi level (Figure 10) and a minimum in case it lies above or in the vicinity of the Fermi level. The effect is getting more pronounced for smaller and smaller temperatures.

The generalization of the infinite- U DSO to the case of different energies $E_{\uparrow} \neq E_{\downarrow}$ is straightforward. One obtains the tunneling rates

$$\Gamma_{l\sigma}^{\pm} = \frac{2\pi}{\hbar} \int d\varepsilon \frac{\alpha_l^{\pm}(\varepsilon) (\alpha(\varepsilon) + \alpha^+(\varepsilon + E_{\bar{\sigma}\sigma}))}{\pi^2 (\alpha(\varepsilon) + \alpha^+(\varepsilon + E_{\bar{\sigma}\sigma}))^2 + (\varepsilon - E_{\sigma 0} + p_{\alpha}(\varepsilon) + p_{\alpha^+}(\varepsilon + E_{\bar{\sigma}\sigma}))^2}. \quad (12)$$

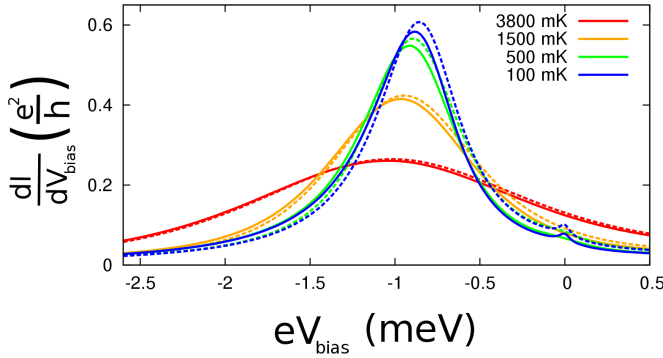


FIG. 10: (Colour online.) The differential conductance versus the bias. We set $E_{10}^{(0)} = E_F - 1\text{meV}$ and chose $\alpha(E_F) = 0.042\text{meV}$, $W = 1\text{eV}$ as in figure 8. We fixed one of the chemical potentials at the Fermi level, $\mu_{l_0} = E_F$, changed only the other one and defined $eV_{bias} = \mu_{l_0} - E_F$. We assumed a capacitive coupling between the leads and the quantum dot in such a way that $E_{10}(V_{bias}) = E_{10}^{(0)} + 0.2eV_{bias}$. We see a resonance appearing at zero bias for small temperatures. The dashed lines show the result of the RTA. The resonance is becoming more and more pronounced with decreasing temperature as it is observed in experiments¹¹. The shape of the curve depends on the capacitive coupling and on how the window between the two chemical potentials is opened; however, the appearing of the zero bias anomaly does not in principle depend on these choices as one can conclude from the fact that they are irrelevant for the differential conductance at zero bias.

We see (Figure 11) that the zero bias anomaly is split according to $eV_{bias} \approx \pm E_{\uparrow\downarrow}$, in agreement with theoretical results^{28,31} and experiments^{8,30}.

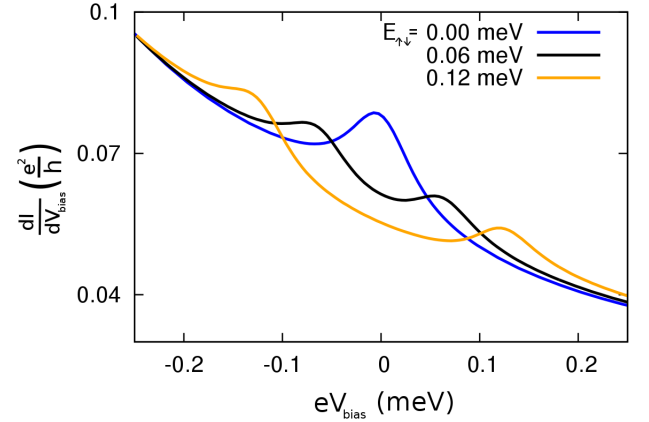


FIG. 11: The zero bias resonance is split up if $E_{\uparrow} \neq E_{\downarrow}$. We chose the temperature $T = 100\text{mK}$ and the remaining parameters as in figure 10 apart from the splitting, $E_{\sigma 0}^{(0)} = E_F - 1\text{meV} \pm E_{\sigma\bar{\sigma}}/2$.

D. Situations in which only one resonance is expected

In Ref.⁸ a resonance close to zero bias whose position changed slightly with the gate voltage was reported. The dependence of the position on the gate voltage was explained by the conjecture that two different wave-functions (not only two different spins) might be involved, such that the assumption of different capacitive couplings of the levels to the gate electrode was justified. However, in this case one would expect to see a second peak at the opposite bias. This was not measured. We assume different capacitive couplings of the levels to the leads and obtain that with growing asymmetry one of the

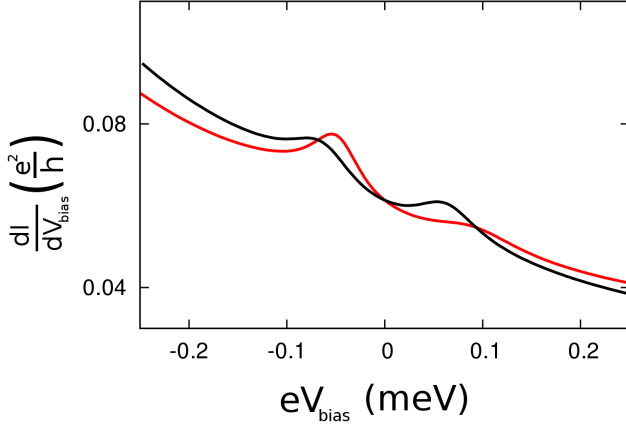


FIG. 12: An asymmetry of the capacitive couplings of the levels to the leads has the effect that the resonances become asymmetric; one is starting to vanish, the other one is getting sharper. The black line is the one already appearing in figure 11. For the red (grey) line we changed the capacitive couplings in such a way that $E_{\uparrow 0}(V_{bias}) = E_{\uparrow 0}^{(0)} + 0.4eV_{bias}$, $E_{\downarrow 0}(V_{bias}) = E_{\downarrow 0}^{(0)} + 0.1eV_{bias}$.

peaks is changing position, getting wider and much less pronounced. The other one, however, is getting sharper (figure 12). The explanation for this behavior at the level of the transition rates, Eq. (12), is that $\Gamma_{l\sigma}^{\pm}$ changes considerably with the bias in regions where

$$\mu_l - \mu_{\bar{l}} \approx E_{\sigma\bar{\sigma}},$$

since then the region of large values of $p_{\alpha_l^+}(\varepsilon - E_{\sigma\bar{\sigma}})$ is leaving or entering the interval over which the integral

$$\Gamma_{l\sigma}^{\pm} = \frac{2\pi}{\hbar} \int d\varepsilon \frac{\alpha_{l\sigma}^{\pm}(\varepsilon) (\alpha_{\sigma}(\varepsilon) + \alpha_{\bar{\sigma}}^{\pm}(\varepsilon + E_{\sigma\bar{\sigma}}))}{\pi^2 (\alpha_{\sigma}(\varepsilon) + \alpha_{\bar{\sigma}}^{\pm}(\varepsilon + E_{\sigma\bar{\sigma}}))^2 + (\varepsilon - E_{\sigma 0} + p_{\alpha_{\sigma}}(\varepsilon) + p_{\alpha_{\bar{\sigma}}^{\pm}}(\varepsilon + E_{\sigma\bar{\sigma}}))^2}. \quad (13)$$

The rates $\Gamma_{l\sigma}^{\pm}$ change rapidly with the bias in regions where

$$\mu_{l\sigma} - \mu_{l'\bar{\sigma}} \approx E_{\sigma\bar{\sigma}}.$$

This leads to the resonance condition

$$eV_{bias} \approx E_{\uparrow\downarrow}^* := E_{\uparrow}^* - E_{\downarrow}^*, \quad (14)$$

where we used the definition $E_{\sigma}^* := E_{\sigma 0} - \mu_{l_0\sigma}$. Indeed, a plot of the differential conductance as function of the bias displays one resonance located approximately at this value of the bias (Fig. 13). Experiments with a pseudo-spin¹ might be interpreted by the use of the SIAM. The DSO predicts the appearing of only one resonance in case only one of the voltages is varied.

essentially goes. This leads to the condition “ $eV_{bias} \approx \pm E_{\uparrow\downarrow}^*$ ” for rapid change of the current with the bias. In case of different capacitive couplings of the levels to the leads the energy difference becomes a function of the bias. With increasing bias, one of the differences is decreasing while the other one is increasing. Thus, one of the resonances is getting sharper while the other one is smeared out. The positions are no longer symmetric with respect to zero bias.

Moreover, we notice that also asymmetric tunnel coupling can have the effect that one of the resonances is getting less pronounced. One can let the coupling functions $\alpha_l(\varepsilon)$, Eq. (3), be dependent on the spin as well as on the lead and thus obtain further independent parameters. We evaluated the differential conductance also in this case (not shown) and we can qualitatively confirm the assumption that different tunnel couplings of the levels to source and drain, too, can be responsible for the observation of only one peak⁸.

As suggested in Ref.⁴⁷, we consider a second situation where the DSO yields, this time, *in principle* only one resonance: The energies $E_{\uparrow}, E_{\downarrow}$ are different and there are four different, separately variable, chemical potentials $\mu_{l\sigma}$ for each of the leads and each of the spins. The chemical potentials of the down-spin are kept constant and equal, $\mu_{l\downarrow} =: \mu_{\downarrow}$; one of the up-spin chemical potentials, too, is kept constant. Only $\mu_{\bar{l}_0\uparrow}$ is varied. The current is considered as a function of $eV_{bias} = \mu_{\bar{l}_0\uparrow} - \mu_{l_0\uparrow}$. The DSO can be easily applied to such a situation. The initial density matrix of the contacts factorizes into four instead of two components. The coupling functions become spin-dependent. The tunneling rates of the infinite- U DSO read in the most general case:

A further in principle possible experiment with pseudo-spin would be the following: The two differences $\mu_{l\uparrow} - \mu_{l\downarrow}, l = l_0, \bar{l}_0$, are held constant and equal. The two voltages $\mu_{\bar{l}_0\sigma} - \mu_{l_0\sigma} =: eV_{bias}$ are equal and are varied. This corresponds so far to an experiment with real spin. The DSO yields two resonances at voltages $eV_{bias} \approx \pm E_{\uparrow\downarrow}^*$. However, the current can be viewed as the sum of the two spin-currents, i.e., the current of the \uparrow -electrons plus the current of the \downarrow -electrons. An advantage of an experiment with pseudo-spin is that, in principle, the two currents can be measured separately. In the theory, anyway, it is not a problem to consider the two components separately. The application of the DSO yields in this situation two resonances of each of the two spin-components

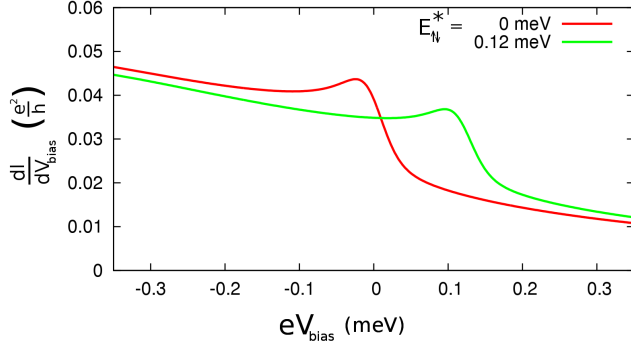


FIG. 13: The differential conductance as function of the bias in the following situation: The temperature is $T = 100mK$, the capacitive coupling we chose to be zero; moreover, we chose $\mu_{\downarrow} = E_F - 0.5meV$, $\mu_{\uparrow} = E_F + 0.5meV$. The energies are chosen as: $E_{\sigma 0} = \mu_{\downarrow\sigma} - 1meV + E_{\sigma\bar{\sigma}}^*/2$.

of the current. To conclude the discussion of the behavior of the resonance obtained by the DSO under various conditions, we can say that the predictions of the DSO are in agreement with those obtained by a purely qualitative approach⁴⁷. Apart from this, the predictions of the DSO are, up to our knowledge, novel.

VII. LINEAR CONDUCTANCE AT FINITE U

In this section we investigate the linear conductance at finite interaction according to Eq. (10). By considering the integrals we can see qualitatively that we can expect an enhancement of the conductance with decreasing temperature if E_{10} lies below and E_{21} lies above the Fermi level: The function $\frac{-1}{k_B T} f' \left(\frac{\varepsilon - E_F}{k_B T} \right)$ of ε has total weight one and is concentrated in a region of the size of the thermal energy around the Fermi level. In the denominators (Eq. (7)) the behaviour of the p -functions becomes important. The principal part $p_h(\varepsilon)$, Eq. (9), measures an asymmetry of the function h with respect to ε (h is an arbitrary function here). In particular, $p_{\alpha+}$ takes negative values around the Fermi level since in this region $\alpha^+(\varepsilon)$ is decreasing (figure 14).

If we decrease the temperature, then the decay of the values of α^+ will be more rapid and thus the absolute values of $p_{\alpha+}(\varepsilon)$ are getting larger. Around the Fermi level, $\varepsilon + p_{\alpha+}(\varepsilon)$ approaches the energy difference E_{10} and the integral increases. At some point the sum even reaches and crosses the level position and then the integral decreases again. For the other integral the arguments are analogous. The energy correction $p_{\alpha-}$ is positive here and increases if we decrease the temperature.

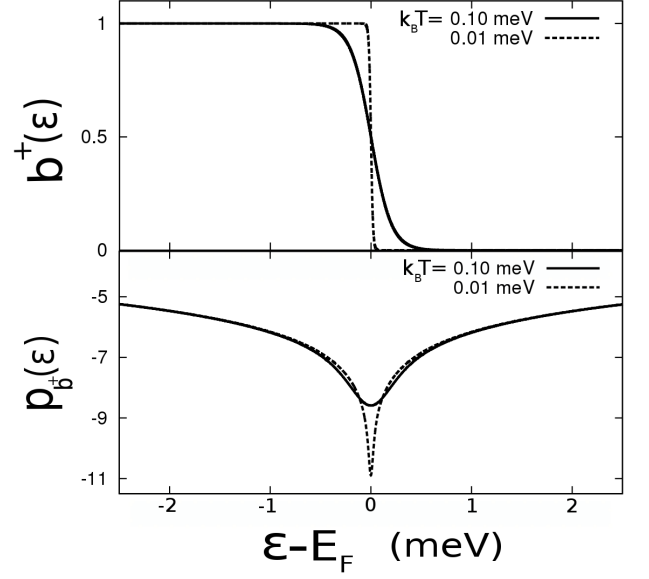


FIG. 14: Behaviour of the normalized function $b_T^+ := \alpha^+(\varepsilon)/\alpha(E_F)$ for which we use the abbreviation b_T^+ and the resulting behaviour of the function $p_{b_T^+}(\varepsilon) := \int d\omega (b_T^+(\varepsilon + \omega) - b_T^+(\varepsilon - \omega))/\omega$ around the Fermi level. It measures the surplus of electrons with energy larger than ε with a strong emphasis on the situation locally around ε . Therefore, the principal parts display a dip around E_F . If we decrease the temperature by a factor of ten, then the value of the principal part in the centre goes down by the logarithm of ten. Moreover, if we stretch the narrower of the two dips by this factor, then we obtain the other dip. There is a well defined universal shape of the dips as we will show in the appendix.

A. DSO-Conductance from weak to strong coupling

For the numerical implementation of Eq. (10) we wrote the coupling functions $\alpha(\varepsilon)$ still as $\alpha(E_F)b(\varepsilon)$, where the choice of $b(\varepsilon)$ is given in figure 7. We modeled the cases of strong and weak tunnel coupling by large and small factors $\alpha(E_F)$, respectively. In figure 15 we show plots of $G^{DSO}(E_{10})$ for different values of the tunnel coupling. In the limit of weak coupling we reproduce the result of the second order theory while for increased coupling we expect essentially three effects: The peaks are getting higher, broader and the maxima are moving towards each other.

For strong coupling and for values of $E_{10} \approx E_F - U/2$ we expect irreducible tunneling processes outside the DSO-approximation to become more relevant: The population of all of the four possible states of the quantum dot is of the order of one here. Hence, processes which transfer $|0\rangle\langle 0|$ into $|2\rangle\langle 2|$ or vice versa or $|\sigma\rangle\langle\sigma|$ into $|\bar{\sigma}\rangle\langle\bar{\sigma}|$ should become more relevant. This might be an explanation for the failure of our diagram selection in describing this regime of parameters.

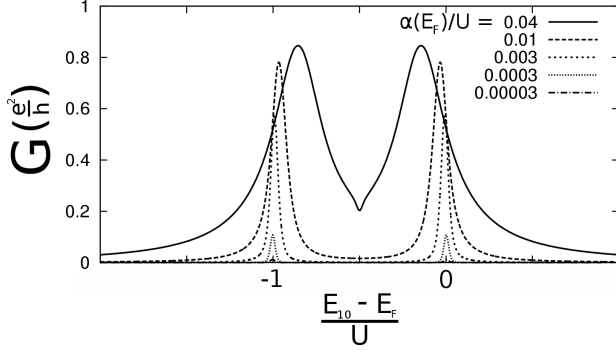


FIG. 15: Plots of the differential conductance at zero bias as a function of E_{10} (corresponding to a plot as a function of the gate voltage) for different tunnel couplings. We chose the interaction to be $U = 1\text{meV}$ and the temperature $T = 100\text{mK}$. For weak coupling we see peaks of small height whose width is given by the temperature; the peak positions are quite precisely defined by the resonance conditions $E_{10} = E_F$ and $E_{21} = E_F$. For increased coupling the corrections are becoming more and more important; the width is increasing with $\alpha(E_F)$, the peak position is shifted by the corrections $p_{\alpha\pm}$. The DSO approximation breaks for strong couplings where it produces a strange sharp dip in the centre of this plot which is not observed in reality.

B. From the empty orbital regime to the Kondo regime

We want to compare now the result of the DSO for the linear conductance as a function of E_{10} and of the temperature with experimental data⁷. In the experiment a region within a two dimensional electron gas was isolated by electrostatically generated tunneling barriers. In this way a quantum dot which is tunnel coupled to leads was formed. Via a gate voltage it is possible to vary E_{10} . The linear conductance was measured as a function of the gate voltage and the temperature. The results were interpreted in terms of the SIAM. The authors distinguish between three different regimes of parameters, depending on whether the level position, i.e., E_{10} is far below the Fermi energy (here the particle number is one, “Kondo regime”), in the vicinity of the Fermi level (“mixed valence regime”) or above the Fermi level (here the particle number is zero, “empty orbital regime”). We tested the performance of the DSO approximation by adjusting the parameters and comparing with the experimental data.

We fitted the parameters in the following way: The temperatures are given explicitly. The value of the Coulomb interaction U , too, we take directly from the experiment. To fix the coupling parameter $\alpha(E_F)$ we plotted $G(E_{10})$ for various values of it. We determined the parameter by the demand that the full width at half maximum of the peaks is close to the measured values (figure 16).

In figure 17 we show a plot of the linear conductance as a function of the energy difference E_{10} for different tem-

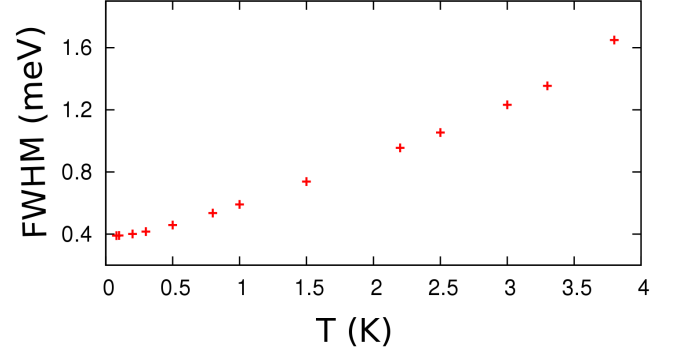


FIG. 16: A plot of the full widths at half maximum (“FWHM”) of the peaks in figure 17 as a function of the temperature; the value of $\alpha(E_F)$ is here 0.042meV . For small temperatures the FWHM seems to saturate at a value of about 0.39meV which is in agreement with the value of the experiment⁷. For large temperatures the FWHM increases; the graph has positive curvature which is happening since the two peaks are getting mixed as we increase the temperature. This is why we cannot define the coupling constant in the same way as done in the experiment: There a linear dependence of the FWHM on the temperature for large temperatures was observed and the coupling constant was determined via the slope of the plot.

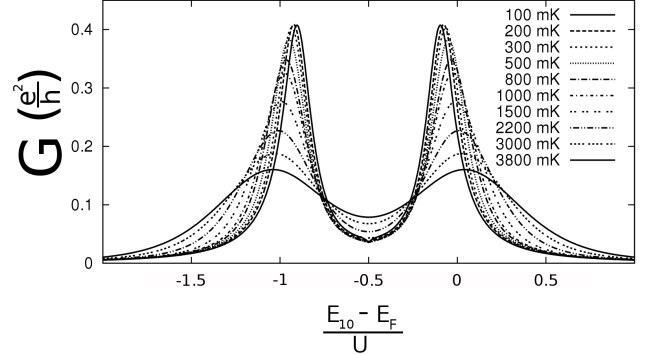


FIG. 17: A plot of the linear conductance as a function of the energy difference E_{10} which corresponds to a plot as a function of the gate voltage. We chose the interaction $U = 1.9\text{meV}$, the coupling $\alpha(E_F) = 0.042\text{meV}$, and the temperatures in agreement with the experiment⁷; the asymmetry of the tunnel couplings to left and right lead we chose as $4\kappa_l\kappa_{\bar{l}} = 0.5$, i.e., we assume an asymmetry of about $\kappa_l : \kappa_{\bar{l}} = 0.17$. For even smaller temperatures we would again see the sharp dip in the centre of the plots already shown in figure 15.

peratures. We get qualitatively very similar behaviour as in⁷. With decreasing temperature, the peaks are moving towards each other, they are getting higher and their widths are getting smaller and seem to saturate finally. In the end, we adjusted also the factor $4\kappa_l\kappa_{\bar{l}}$ which expresses an asymmetry of the tunneling couplings to source and drain. This, however, is only a fit made in such a way that

the absolute values of the linear conductance are about the same in theory and experiment. The experiment was addressed also by Ref.⁴⁸ where a different asymmetry was assumed and good quantitative agreement was obtained. Therefore, it is difficult to formulate exact rules defining in what regime of parameters the DSO is quantitatively correct.

For a further comparison we show the dependence of G on the temperature for fixed E_{10} . In order to do this we express E_{10} in terms of its position relative to the Fermi level and divide it by some quantity Γ which characterizes the tunnel coupling in a similar way as in the experiment. By the plot we conclude that we have agreement of our

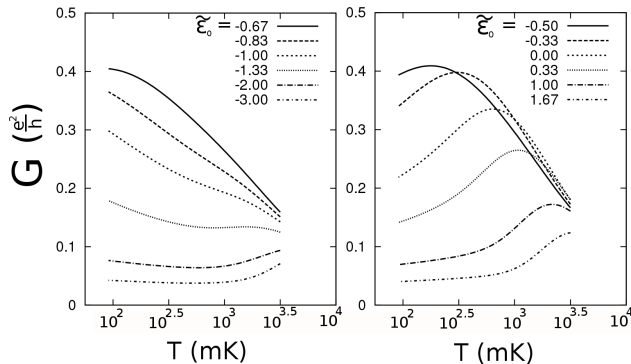


FIG. 18: A plot of $G(T)$ for fixed values of the gate voltage, expressed in terms of $\tilde{\varepsilon}_0 := (E_{10} - E_F)/\Gamma$. Here we take $\Gamma \approx 0.3 \text{ meV}$ as in the experiment with the argument that the saturation width of figure 16 is the same as in the experiment. The different parameter regimes are called "empty orbital regime" ($\tilde{\varepsilon}_0 > 0$), "mixed valence regime" ($-0.5 < \tilde{\varepsilon}_0 < 0$) and "Kondo regime" ($\tilde{\varepsilon}_0 \ll -0.5$).

theoretical result with the experimental data in the sense that the transition from the empty orbital regime, where with decreasing temperature we see only a decrease and then rather constant behaviour, to the Kondo-regime, where we see only an increase, happens within an interval of E_{10} -values of the size of about 2Γ .

On the other hand, we see a qualitative deviation in the regime $E_{10} \approx E_F$: The G obtained by the DSO displays quite clearly a decrease with decreasing temperatures for small temperatures while in the experiment this decrease is much weaker. A study of the behaviour of the linear conductance in all three different regimes obtained by numerical renormalization-group calculations can be found in Ref.⁴⁹.

VIII. CONCLUSIONS

We used a diagrammatic approach in order to describe transport across a SIAM quantum dot. We found a minimum selection of diagrams which we called "dressed second order" (DSO) diagrams, which straightforwardly

yield the current in terms of transition rates. In general, the DSO represents the natural extension of the sequential tunneling approximation, valid for large interactions and when $k_B T \gg \Gamma$, to the regime $k_B T \sim \Gamma$. In particular, the conductance versus gate voltage exhibits peaks with a broadening no more given by the temperature but by the tunnel coupling. Appealing of the DSO is its simplicity and its potential for scalability to multilevel quantum dot systems. Moreover, its extension to set-ups with ferromagnetic or superconducting leads is straightforward.

Furthermore, the diagram selection contains a zero bias anomaly developing at low temperatures. We showed that, if the degenerate level lies below the Fermi energy, then it is a zero bias maximum of the differential conductance which appears for low temperatures and is getting more pronounced if the temperature is decreased further. This is in qualitatively good agreement with experiments^{8,11}.

We showed that the anomaly displays features of the Kondo effect such as a universality in the dependence of the linear conductance as function of the temperature. We investigated the behaviour of the anomaly in case a magnetic field is applied and discussed the impact of asymmetries with respect to capacitive or tunnel couplings to the leads. Moreover, we considered a situation where we expect in principle only one peak.

We pointed out the close relation of the DSO diagram selection to that of the resonant tunneling approximation (RTA) and compared their results in the case of infinitely large interaction. The RTA is more precise in the sense that it includes more diagrams; however, the DSO can be applied more easily to the case of energetically split levels. We showed that the inclusion of the diagrams outside the DSO which are contained in the RTA is not essential to the appearing of the zero bias anomaly. We think we found the smallest possible selection which contains the anomaly.

Finally, we applied the approximation in the case of finite interaction and compared its result at the level of the linear conductance with an experiment, Ref.⁷. We found good qualitative agreement with the experimental data. It is difficult to formulate general rules defining for what regime of parameters the DSO approximation is quantitatively correct. Being an extension of the sequential tunneling approximation, we expect the DSO to well cover the regime of large interactions down to temperatures $k_B T \sim \Gamma$. Obvious failure of the approximation in describing the experiment⁷ we observed in the region $E_{10} \approx 1/2(E_F + E_F - U)$ for small temperatures.

The DSO for finite U does not produce the observed plateau of the linear conductance as a function of the gate voltage for small temperatures forming between the two resonances¹¹. Additionally, the DSO for finite U does not correctly describe the noninteracting, spin degenerate limit. There is, however, a natural extension of the DSO which is indeed doing so, as outlined in Sec. V. Thus, there is hope that the DSO can be improved in such a

way that the case of small interaction is described better. Moreover, the same class of diagrams could provide a natural way to extend the RTA to finite interaction as described by figure 6.

In conclusion, the DSO is a novel approximation for the intermediate coupling regime which can additionally provide useful insight also at temperatures $k_B T \ll \Gamma$.

IX. ACKNOWLEDGEMENTS

We thank the DFG for financial support within the framework of the GRK 1570 and the SFB 689.

Appendix

We want to derive a representation

$$\int d\varepsilon \frac{\pi^2 \alpha^2(\varepsilon)}{d(\varepsilon)} \Big|_{V_{bias}=0} \frac{-1}{k_B T} f' \left(\frac{\varepsilon - E_F}{k_B T} \right) \\ \approx F^{RTA} \left(\frac{E_{10} - \bar{E}_{10}}{\alpha(E_F)}, \frac{k_B T}{\alpha(E_F)} \right),$$

where the denominator of the integral is given by $d(\varepsilon) := \pi^2(\alpha + \alpha^+)^2(\varepsilon) + (\varepsilon + p_{\alpha+\alpha^+}(\varepsilon) - E_{10})^2$, the function F^{RTA} is universal and where \bar{E}_{10} does not depend on the gate voltage or on the temperature. To this end we write the second order function $\alpha(\varepsilon)$ as $\alpha(E_F)b(\varepsilon)$ and divide numerator and denominator of the integral by $\alpha(E_F)$. Moreover, we write $\varepsilon = E_F + xk_B T$ and integrate with respect to x instead of ε . We argue then that the integral is concentrated in a region of a few multiples of the thermal energy around E_F and that it is, because of this, for sufficiently small temperatures allowed to estimate $b(\varepsilon) = 1$ and $p_b(\varepsilon) = p_b(E_F)$; $p_b(E_F)$ is zero because we chose the function b to be symmetric around E_F . After these modifications we obtain the integral:

$$\int dx \frac{-\pi^2 f'(x)}{\pi^2(1 + f(x))^2 + \phi^2(x)}, \quad (15)$$

where we used the abbreviation

$$\phi(x) := x \frac{k_B T}{\alpha(E_F)} + \frac{E_F - E_{10}}{\alpha(E_F)} + p_{b_T^+}(E_F + xk_B T)$$

and where the function b_T^+ is given by $b_T^+(\varepsilon) = b(\varepsilon)f((\varepsilon - E_F)/k_B T)$.

Thus, what remains to be done is the analysis of $p_{b^+}(E_F + xk_B T)$. First of all, we consider its values in $x = 0$ for different temperatures. By taking the derivative with respect to the temperature one obtains:

$$\frac{d}{dT} \int_0^\infty \frac{b(E_F + \omega)f\left(\frac{\omega}{k_B T}\right) - b(E_F - \omega)f\left(\frac{-\omega}{k_B T}\right)}{\omega} \\ = \frac{1}{T} \int_0^\infty dx - f'(x) [b(E_F + xk_B T) + b(E_F - xk_B T)] \\ \approx \frac{1}{T}.$$

For the final estimate we assumed that the temperature is sufficiently small such that in a region of a few $k_B T$ around the Fermi level we have $b(\varepsilon) \approx 1$.

Secondly, we need to consider the values of $p_{b^+}(E_F + xk_B T)$ for *one* temperature and different values of x . We consider

$$p_{b_T^+}(E_F + xk_B T) - p_{b_T^+}(E_F) = \quad (16)$$

$$\int_0^\infty \frac{dy}{y} (b(E_F + k_B T(x+y))f(x+y) \\ - b(E_F + k_B T y)f(y) \\ - b(E_F + k_B T(x-y))f(x-y) \\ + b(E_F - k_B T y)f(-y)).$$

For every single value of y , the limit $T \rightarrow 0$ can be taken. We can guess that the limit of the integral is given by the integral of the point-wise limit,

$$g(x) := \int_0^\infty \frac{dy}{y} (f(x+y) - f(y) \\ - f(x-y) + f(-y)). \quad (17)$$

Then we replace the function of x given by Eq. (16) by $g(x)$ with the argument that for small temperatures the deviations between the two can be expected to be small.

For the proof we want to apply Lebesgue's convergence theorem, so we need an integrable upper bound which is independent of the temperature. Moreover, we write $\int_0^\infty = \int_0^1 + \int_1^\infty$ since the different intervals make different treatment necessary.

The integrand has the form

$$(AB)(x+y) - (AB)(y) - (AB)(x-y) + (AB)(-y).$$

As to the integral \int_0^1 , we group the terms with equal " x " into pairs and consider the two resulting differences separately. By adding and subtracting the mixed terms $A(x+y)B(x-y)$ one can see that we have even a constant upper bound within this interval. The conditions which we demand from the function $b(\varepsilon)$ for this are the following:

- It is bounded, $|b(\varepsilon)| \leq B$, B independent of ε .
- It satisfies a Lipschitz condition of the form: $|b(\varepsilon) - b(\varepsilon')| \leq L|\varepsilon - \varepsilon'|$, L independent of ε and ε' .

We mention that the Fermi function, too, has the two properties; the latter can be seen by using the fact that the derivative of the Fermi function is bounded and the mean value theorem. Moreover, a Lorentzian or our choice of the function b (figure 7) fulfills these conditions.

As to the integral \int_1^∞ , we group the terms with equal sign in front of y into pairs. Again, it is useful to add and subtract the mixed terms, e. g., $A(x+y)B(y)$. We

obtain then:

$$\begin{aligned} & \frac{1}{y} b(E_F + k_B T(x + y)) (f(x + y) - f(y)) + \\ & \frac{1}{y} (b(E_F + k_B T(x + y)) - b(E_F + k_B T y)) f(y). \quad (18) \end{aligned}$$

The point-wise limit of the first line is $1/y (f(x + y) - f(y))$, and the convergence is bounded by $B/y |f(x + y) - f(y)|$. This is integrable because we can estimate:

$$\begin{aligned} \frac{|f(x + y) - f(y)|}{y} & \leq \max \{|f'(z)| : |z - y| \leq |x|\} |x| \\ & =: m_x(y) |x|, \end{aligned}$$

where we used $y \geq 1$. We treat x as a constant during these considerations. Because of the rapid decay of the derivative of the Fermi function $m_x(y)$ is integrable.

The point-wise limit of the second line is zero. In order to get an integrable upper bound we introduce the function

$$L_{>}(\varepsilon) := \sup \left\{ \frac{|b(\varepsilon'') - b(\varepsilon')|}{\varepsilon'' - \varepsilon'} : \varepsilon \leq \varepsilon' < \varepsilon'' \right\}.$$

Then we can estimate the second line by

$$\begin{aligned} & \left| \frac{1}{y} (b(E_F + k_B T(x + y)) - b(E_F + k_B T y)) f(y) \right| \\ & \leq \frac{|x|}{y^2} [E_F + k_B T(y - |x|) - E_F + k_B T|x|] \\ & L_{>}(E_F + k_B T(y - |x|)), \end{aligned}$$

where we multiplied and divided everything by $k_B T |x| y$. (The square bracket is just a complicated way of writing “ $k_B T y$ “.) We note now that for sure $L_{>}(\varepsilon) \leq L$ and make the further assumption that the function $\varepsilon L_{>}(\varepsilon)$ is bounded over any interval which has a lower bound, i.e., for any ε_0 we have

$$L_{>}(\varepsilon_0) := \sup \{ \varepsilon L_{>}(\varepsilon) : \varepsilon \geq \varepsilon_0 \} < \infty. \quad (19)$$

This assumption is fulfilled both for Lorentzian shapes of $b(\varepsilon)$ and for our way of choosing the second order function (figure 7), the reason being the rapid decay of the derivatives of these functions. Using these properties we obtain for temperatures smaller than some arbitrary temperature T_0 the upper bound:

$$\frac{|x|}{y^2} \{ L (|E_F| + |x| k_B T_0) + L_{>} (E_F - |x| k_B T_0) \}.$$

This is integrable with respect to y over the interval between one and infinity and independent of the temperature between zero and T_0 . With Lebesgue we can conclude that the integral of the function (18) of y really goes to zero. The terms with a minus in front of y we can treat in the same way. For this we introduce functions $L_{<}(\varepsilon)$ and $L^<(\varepsilon)$ in analogy to the above method and demand the corresponding property of $b(\varepsilon)$ of assumption (19).

We showed the convergence

$$p_{b_T^+}(E_F + k_B T x) - p_{b_T^+}(E_F) \rightarrow g(x) \quad (T \rightarrow 0)$$

for arbitrary x , where the limit is given by the definition

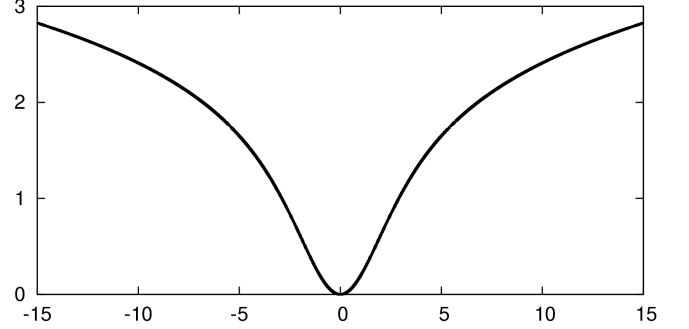


FIG. 19: A plot of the function $g(x)$ defined by eq. (17), i.e., the normalized shape of the functions $p_{b_T^+}(\varepsilon)$ around the Fermi level in units of the thermal energy. The growth of $g(x)$ is logarithmic in the sense that $xg'(x) \rightarrow 1$ ($|x| \rightarrow \infty$). However, because of the presence of the derivative of the Fermi function in the integrals, the behaviour of $g(x)$ around $x = 0$ is more important for us.

(17). In figure 19 we plotted the function $g(x)$. Already earlier we noticed that the dependence of $p_{b_T^+}(E_F)$ on the temperature is logarithmic. By putting the two pieces of information together we can estimate:

$$p_{b_T^+}(E_F + x k_B T) \approx p_{b_{T_{\alpha(E_F)}}^+}(E_F) + \log \left(\frac{T}{T_{\alpha(E_F)}} \right) + g(x),$$

where $T_{\alpha(E_F)}$ is defined by the condition $k_B T_{\alpha(E_F)} = \alpha(E_F)$. We insert this into the integral (15) and obtain:

$$\begin{aligned} \phi(x) & \approx x \frac{T}{T_{\alpha(E_F)}} + \log \left(\frac{T}{T_{\alpha(E_F)}} \right) + g(x) \\ & + \frac{E_F - E_{10}}{\alpha(E_F)} + p_{b_{T_{\alpha(E_F)}}^+}(E_F). \end{aligned}$$

Now we define a reference value for E_{10} , “ \bar{E}_{10} ”, by the demand that the value of the second line is zero for $E_{10} = \bar{E}_{10}$. The integral (15) has then the form

$$F^{RTA} \left(\frac{E_{10} - \bar{E}_{10}}{\alpha E_F}, \frac{k_B T}{\alpha(E_F)} \right),$$

where the definition of F^{RTA} is

$$F^{RTA}(a, b) = \int dx \frac{-\pi^2 f'(x)}{\pi^2 (1 + f(x))^2 + \phi_{a,b}^2(x)}$$

with

$$\phi_{a,b}(x) = g(x) - a + xb + \log(b). \quad (20)$$

The corresponding integral in the formula for the linear conductance within the DSO in the infinite-U case can be represented in an analogous way. The difference is that in the numerator we get $-\pi^2 f'(x)(1 + f(x))$ instead of only $-\pi^2 f'(x)$.

-
- * Electronic address: `johannes.kern@physik.uni-regensburg.de`
- ¹ U. Wilhelm, J. Schmid, J. Weis, K.v. Klitzing, *Physica E* **14**, 385 (2002).
 - ² P.W. Anderson, *Phys. Rev.* **124**, 41 (1961).
 - ³ *Single Charge Tunneling*, edited by H. Grabert and M.H. Devoret (Plenum, New York 1992).
 - ⁴ *Mesoscopic Electron Transport*, edited by L.L. Sohn, L.P. Kouwenhoven and G. Schön, NATO ASI Series **345**, (1996).
 - ⁵ J. Kondo, *Progr. Theor. Phys.* **32**, 37 (1964).
 - ⁶ D. Goldhaber-Gordon, Hadas Shtrikman, D. Mahalu, D. Abusch-Magder, U. Meirav and M.A. Kastner, *Nature* **391**, 156 (1998).
 - ⁷ D. Goldhaber-Gordon, J. Göres, M.A. Kastner, Hadas Shtrikman, D. Mahalu and U. Meirav, *Phys. Rev. Lett.* **81**, 5225 (1998).
 - ⁸ J. Schmid, J. Weis, K. Eberl and K.v. Klitzing, *Physica B* **256-258**, 182 (1998).
 - ⁹ S.M. Cronenwett, T.H. Oosterkamp and L.P. Kouwenhoven, *Science* **281**, 540 (1998).
 - ¹⁰ W. van der Wiel, S. De Franceschi, T. Fujisawa, J.M. Elzerman, S. Tarucha and L.P. Kouwenhoven, *Science* **289**, 2105 (2000).
 - ¹¹ M. Grobis, I.G. Rau, R.M. Potok, H. Shtrikman and D. Goldhaber-Gordon, *Phys. Rev. Lett.* **100**, 246601 (2008).
 - ¹² J. Nygård, D.H. Cobden and P.E. Lindelof, *Nature* **408**, 342 (2000).
 - ¹³ P. Jarillo-Herrero, J. Kong, H.S.J. van der Zant, C. Dekker, L.P. Kouwenhoven and S. De Franceschi, *Nature* **434**, 484 (2005).
 - ¹⁴ S. Sahoo, T. Kontos, J. Furer, C. Hoffmann, M. Graber, A. Cottet and C. Schönenberger, *Nat. Phys.* **1**, 99 (2005).
 - ¹⁵ J.R. Hauptmann, J. Paaske and P.E. Lindelof, *Nature Phys.* **4**, 373 (2008).
 - ¹⁶ M. Gaass, A.K. Hüttel, K. Kang, I. Weymann, J. von Delft and C. Strunk, *Phys. Rev. Lett.* **107**, 176808 (2011).
 - ¹⁷ S. Csonka, L. Hofstetter, F. Freitag, S. Oberholzer, C. Schönenberger, T.S. Jespersen, M. Aagesen and J. Nygård, *Nano Lett.* **8**, 3932 (2008).
 - ¹⁸ A.V. Kretinin, H. Shtrikman, D. Goldhaber-Gordon, M. Hanl, A. Weichselbaum, J. von Delft, T. Costi and D. Mahalu, *Phys. Rev. B* **84**, 245316 (2011).
 - ¹⁹ A.N. Pasupathy, R.C. Bialczak, J. Martinek, J.E. Grose, L.A.K. Donev, P.L. McEuen and D.C. Ralph, *Science* **306**, 86 (2004).
 - ²⁰ D.V. Averin, A.N. Korotkov and K.K. Likharev, *Phys. Rev. B* **44**, 6199 (1991).
 - ²¹ C.W.J. Beenakker, *Phys. Rev. B* **44**, 1646 (1991).
 - ²² M.A. Reed, C. Zhou, C.J. Muller, T.P. Burgin and J.M. Tour, *Science* **278**, 252 (1997).
 - ²³ E. Lörtscher, H.B. Weber and H. Riel, *Phys. Rev. Lett.* **98**, 176807 (2007).
 - ²⁴ A. Cottet and M.S. Choi, *Phys. Rev. B* **74**, 235316 (2006).
 - ²⁵ S. Koller, M. Grifoni and J. Paaske, *Phys. Rev. B* **85**, 045313 (2012).
 - ²⁶ L.I. Glazman and M.E. Raikh, *Pis'ma Zh. Eksp. teor. Fiz.* **47**, 378 (1988) [*JETP Lett.* **47**, 452 (1988)].
 - ²⁷ T.K. Ng and P.A. Lee, *Phys. Rev. Lett.* **61**, 1768 (1988).
 - ²⁸ Y. Meir, N.S. Wingreen and P.A. Lee, *Phys. Rev. Lett.* **70**, 2601 (1993).
 - ²⁹ N.S. Wingreen and Y. Meir, *Phys. Rev. B* **49**, 11040 (1994).
 - ³⁰ D.C. Ralph and R.A. Buhrman, *Phys. Rev. Lett.* **72**, 3401 (1994).
 - ³¹ J. König, J. Schmid, H. Schoeller and G. Schön, *Phys. Rev. B* **54**, 16820 (1996).
 - ³² H. Schoeller and G. Schön, *Phys. Rev. B* **50**, 18436 (1994).
 - ³³ A. Levy Yeyati, J.C. Cuevas, A. López-Dávalos and A. Martín-Rodero *Phys. Rev. B* **55**, R6137 (1997).
 - ³⁴ J.P. Pekola et al., *Phys. Rev. Lett.* **105**, 026803 (2010).
 - ³⁵ H. Schoeller, Habilitationsschrift, URL: <http://digbib.ubka.uni-karlsruhe.de/volltexte/44097> (1997).
 - ³⁶ N.E. Bickers, *Rev. Mod. Phys.* **59**, 845 (1987).
 - ³⁷ A.D. Gottlieb and L. Wesoloski, *Nanotechnology* **17** R57 (2006).
 - ³⁸ K. Blum, Plenum Press, *Density Matrix: Theory and Applications*, New York (1996).
 - ³⁹ J. Kern, *Workshop Report 2010*, URL: <http://homepages-nw.uni-regensburg.de/kej62310/index/index.html> (2012).
 - ⁴⁰ M. Grifoni, M. Sasseti and U. Weiss, *Phys. Rev. E* **53**, R2033 (1996).
 - ⁴¹ U. Weiss, *Quantum dissipative systems*, World Scientific, Singapore (2012).
 - ⁴² S. Koller, M. Grifoni, M. Leijnse and M.R. Wegewijs, *Phys. Rev. B* **82**, 235307 (2010).
 - ⁴³ N.W. Ashcroft and N.D. Mermin, *Solid State Physics*, W. B. Saunders Company (1976).
 - ⁴⁴ G. Doetsch, R. Oldenbourg Verlag, *Anleitung zum praktischen Gebrauch der Laplace-Transformation und der Z-Transformation*, München (1967).
 - ⁴⁵ J. König, Diplomarbeit, Universität Karlsruhe (1995).
 - ⁴⁶ T.A. Costi, A.C. Hewson and V. Zlatić, *J. Phys. Condens. Matter* **6**, 2519 (1994).
 - ⁴⁷ J. Kern, *Workshop Report 2012*, URL: <http://homepages-nw.uni-regensburg.de/kej62310/index/index.html> (2012).
 - ⁴⁸ H. Schoeller and J. König, *Phys. Rev. Lett.* **84**, 3686 (2000).
 - ⁴⁹ T.A. Costi and V. Zlatić, *Phys. Rev. B* **81**, 235127 (2010).